DETERMINATION OF DETONATION VELOCITY OF EXPLOSIVE COMPOUNDS USING OPTICAL TECHNIQUES

by

Michael Scott Shattuck

Submitted in Partial Fulfillment
of the Requirements for the Degree of
Master of Science in Mechanical Engineering
with Specialty in Explosives Engineering

New Mexico Institute of Mining and Technology
Socorro, New Mexico
January, 2015

ABSTRACT

The detonation velocity of explosives is an important parameter in the field of explosives engineering. It is the speed at which detonation reaction travels through an explosive. The detonation reaction is a combination of a shock wave that initiates the rapid combustion of the material and a reaction zone that supports the shock wave propagation. The detonation velocity of an explosive is directly rated to the power of the detonation and therefore the engineering applications best suited for that particular explosive. There are several ways to measure detonation velocity, but the one of particular interest for this study uses optical techniques to capture images of the shock wave in the air (or surrounding material) created by the explosion. Using these images, one can determine the velocity of the shock wave, and in turn, the detonation velocity. These optical methods are attractive because they are relatively simple to use, inexpensive (provided that the test facility has a high-speed camera), and can be used on a wide variety of scales. The shock wave emitted from the initiation of three different test items is analyzed: shotgun shell primers, NONEL® shock tube, and RP-2 detonators. The velocity of the shock wave at the explosive/air interface is determined from the high-speed camera images and the detonation velocity is ascertained using Rankine-Hugoniot jump equations. The result is compared to published values for the explosive being tested. Results for primers and NONEL® revealed several complications in testing these two items and detonation velocity calculations returned erroneous results. RP-2 detonators test results had a detonation velocity comparable to published values. The use of this optical technique with a standard high-speed camera is plausible under ideal conditions, but there is a large uncertainty in the final measurement.

Keywords: Explosives; Detonation Velocity; Shock Velocity; Schlieren

ACKNOWLEDGMENTS

I would first like to thank the members of my graduate committee, Dr. Lim, Jerome Stofleth, and especially my chairperson, Dr. Hargather, whose guidance and support made this possible. Dr. Hargathers enthusiasm for teaching his students and breadth of knowledge is truly astounding. Next I would like to thank all the professors that taught the classes I attended. They all made learning the material of the course enjoyable and were all very helpful. My lab mates at the New Mexico Tech Shock and Gas Dynamics Laboratory provided a constant source of valuable information and inspiration. Special thanks to Cynthia Romo and Jesse Tobin for their ardent dedication and encouragement throughout the final months of completing my thesis. I would like to thank my family for their inspiration and support during my time at New Mexico Tech. My father taught me the values that I hold dear, and without his support and confidence in me, I have no doubt I would not have achieved my educational goals. My mother was a constant voice of encouragement and had unyielding faith in me throughout my education and my life which has fueled my success. Both my parents and my brother have instilled in me my faith in God, whom I give the most thanks, because in Him, all things are possible.

This thesis was typeset with LaTeX[1] by the author.

[1]The LaTeX document preparation system was developed by Leslie Lamport as a special version of Donald Knuth's TeX program for computer typesetting. TeX is a trademark of the American Mathematical Society. The LaTeX macro package for the New Mexico Institute of Mining and Technology thesis format was written for the Tech Computer Center by John W. Shipman.

CONTENTS

LIST OF TABLES

LIST OF FIGURES

NOMENCLATURE

List of Symbols

ρ	density
ν	specific volume
P	pressure
u	particle velocity
U	shock velocity
e	internal energy
t	time
STP	standard temperature and pressure
a_0	speed of sound in air at STP
C_0	bulk sound speed
s	material constant
D	detonation velocity
TMD	thoretical maximum density
M	Mach number

List of Subscripts

air	air
e	explosive
CJ	Chapman-Jouget state
0	pre-shocked state or STP conditions
1	shocked state

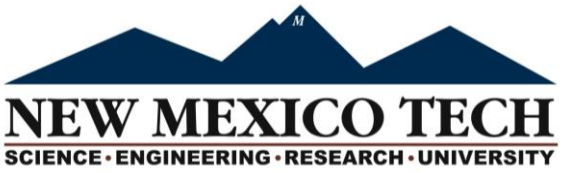

This thesis is accepted on behalf of the faculty
of the Institute by the following committee:

Dr. Michael Hargather

_____

Academic Advisor

Dr. Michael Hargather

_____

Research Advisor

Dr. Seokbin Lim

_____

Committee Member

Jerome Stofleth

_____

Committee Member

_____

Committee Member

I release this document to New Mexico Institute of Mining and Technology

Michael Scott Shattuck January 15, 2015

_____

Student Signature Date

CHAPTER 1

INTRODUCTION AND LITERATURE REVIEW

1.1 Introduction

Explosives are important to the everyday life of the average person. Almost any product that contains metal is made from ore that was likely extracted using explosives. Many commercial products contain metal that was mined, and the mining industry uses about 90% of all explosives produced today. Some nonmetals are also mined, such as the coal that is used to produce about 42% of the nations electrical power [1]. Military uses for explosives are obvious and crucial, but there are hundreds of other uses that may not be as obvious: explosive welding, inflation of airbags in vehicles, avalanche control, opening oil wells, and demolition of structures, among hundreds of other uses. Modern life would not be the same without the use of explosives.

Several parameters characterize the performance of an explosive, but one of particular interest is detonation velocity. It is the speed at which a shock wave detonation reaction travels through an explosive. A detonation reaction is comprised of a shock wave immediately followed by a reaction zone. The shock wave initiates the chemical reaction in the explosive which rapidly changes the explosive compound into its product gases in the reaction zone. The detonation velocity of an explosive is directly rated to the power of the detonation and therefore determines the engineering applications best suited for that particular explosive [2][3]. There are several ways to measure detonation velocity, but the one of interest for this study uses optical techniques to capture images of the shock wave in the air (or surrounding material) created by the explosion. Using these images, one can determine the velocity of the shock wave, and in turn, the detonation velocity [4]. These optical methods are attractive because they are relatively simple to use, inexpensive (provided that the test facility has a high speed camera), and can be used for a wide variety of scales [5] .

The detonation of an explosive creates a shock wave that is propagated through the surrounding medium, and for the purpose of this study, the surrounding medium will always be air. A shock wave (or shock front) is a propagating wave of disturbance in the medium. It is a discontinuous change in state of the material. Across the shock front there is a jump in pressure, temperature, and density in the medium. The shock wave travels at a very high velocity but eventually attenuates to an acoustic wave. Capturing the shock wave as it moves

and causes aberrations in the background scenery is a technique known as background oriented schlieren [6].

It should be noted that the detonation wave in an explosive (usually a solid) is completely different from the shock wave in the medium. The detonation wave in an explosive is the result of, and is driven by, the chemical reaction occurring just behind it. The shock in air is the result of the expansion of gases, and its propagation through the air is no longer being driven by a chemical reaction and is therefore prone to attenuation. It is this difference that creates the difficulty in relating the air shock to the detonation velocity and is an important aspect of this study.

1.2 Detonation Velocity Measurement Methods

Since the 1940s, many methods have been devised to determine the detonation velocity of explosives. Several traditional ways are presented, concluding with the unique optical methods employed for this research.

1.2.1 Estimation of Detonation Velocity

Some methods exist for estimating detonation velocities of explosives that do not require actually detonating the explosive. Instead, if some of the properties are known, such as the chemical composition, density, physical state, and the chemical decomposition equation, then detonation velocity may be estimated. These methods are good starting points for obtaining detonation velocity, and some can be very accurate, while others are not and may have limitations in their use.

An empirical method set forth by Rothstein [7] uses the chemical formula, structure, and physical state of the explosive to calculate detonation velocity at the theoretical maximum density (TMD) of the compound. One must only know the molecular formula, if the compound is aromatic (contains a benzene ring [8]), and whether it is a liquid or solid. A calculation for TNT at a density of 1.64 g/cc is in error by 3.6%. This method is useful for homogeneous explosives at their TMD.

Density has a large effect on detonation velocity, especially the density variations for a single compound. The relation is closely linear for many explosives for a reasonable range of density. Cooper proposes that only two empirical constants that are specific to the explosive compound, a and b in Equation 1.1, are needed to estimate detonation velocity (D) if the density (ρ) is known [8]. The formula is:

$$D = a + b\rho \tag{1.1}$$

It is suggested that the density be within 0.85 of the TMD for this equation to be accurate within 10% to 15%.

One method set forth by Kalmet and Jacobs [9] uses a specific hierarchy for the detonation products to estimate detonation velocity. The chemical reaction equation must be balanced according to this hierarchy and the heats of detonation must be known along with the initial explosive density. Molecular weights must also be calculated to use this lengthy method.

1.2.2 Experimental Measurement of Detonation Velocity

Some methods require actual detonation of explosives and taking measurements from the experiment. These methods are more costly and time consuming, but are more exact, especially for complicated explosive mixtures.

One of the most common methods to measure detonation velocity is with a rate stick, or cylinder test, outlined by Cooper and Kurowski [10]. A copper cylinder is filled with an explosive. The cylinder has pre-drilled holes along its length to hold pressure pin gauges at a known distance apart (Figure 1.1) [11]. The cylinder is detonated from one end and as the detonation progresses down the pipe, the pressure pins are activated and the time recorded by a computer.

Knowing the times and distance between the pins, the velocity can be calculated. Figure 1.1 shows the pressure pins protruding from a clear plastic cylinder for demonstration purposes. Test wires are connected to the pressure pins on one end and an oscilloscope on the other end.

Another prevalent test is the aquarium test. It is basically the cylinder test where the explosive charge is placed in a transparent container full of water. The explosive is typically cylindrical in shape, placed vertically in the container, and detonated from above. As the detonation front travels down the cylinder, the oblique shock wave created by the expanding product gases travels through the water and is easily seen due to the high refractive index of the water (compared to air) [12]. A schematic is shown in Figure 1.2 [12] and a sequence of high-speed photos is shown in Figure 1.3 [13]. A grid is placed in the background to help determine the velocity of the shock wave. This method is attractive because the detonation front in the explosive is easily differentiated from the detonation products because the water acts to contain the product gases [13].

Another common test in the explosives industry is the plate dent test. A measured quantity of explosive is place directly onto a thick steel plate (Figure 1.4) [11]. The detonation forms a dent in the plate and the depth of the dent is directly dependent on the peak pressure of the explosive, and therefore the detonation velocity can be calculated [10][11]. While this method is simple to use, there are no set standards for the parameters of the test, giving way to wildly differing data sets. Some tests use an indenter ball, others use bare explosive charges. Also, the plate may bend becoming dish-shaped, as well as being indented by the ball bearing, making analysis of the results difficult to define [14].

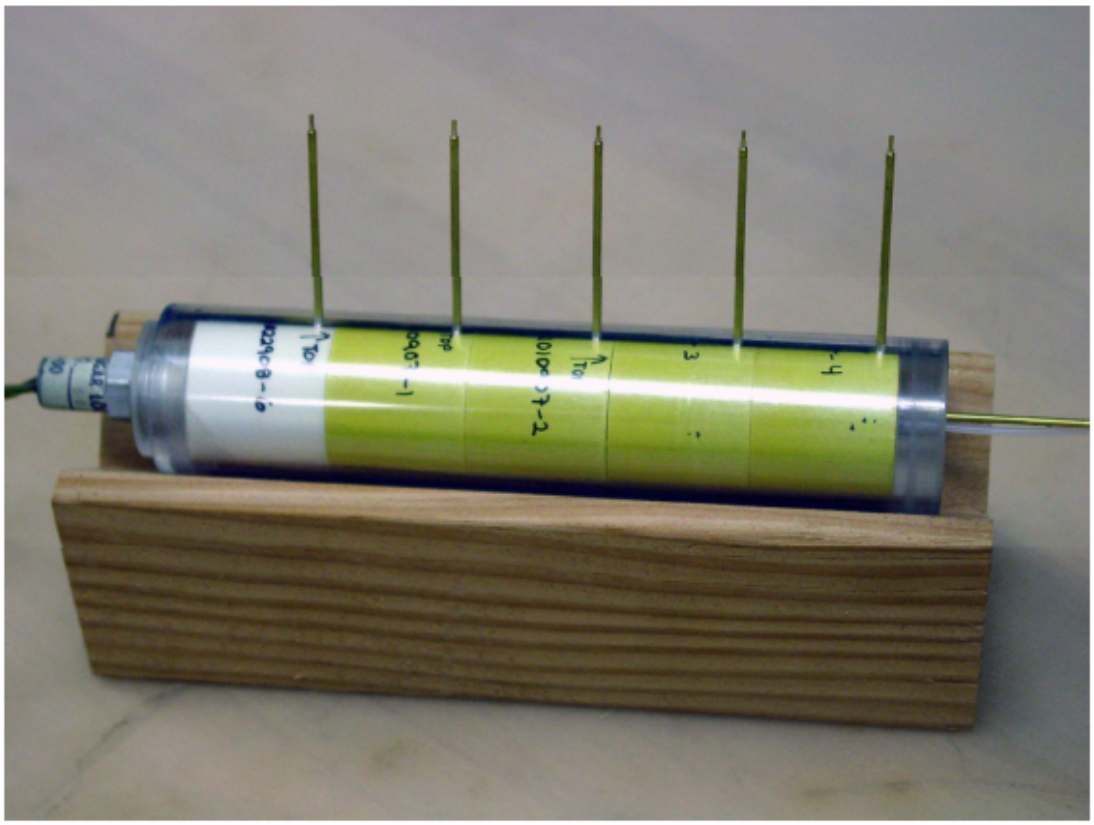

Figure 1.1: Rate stick demonstration cylinder

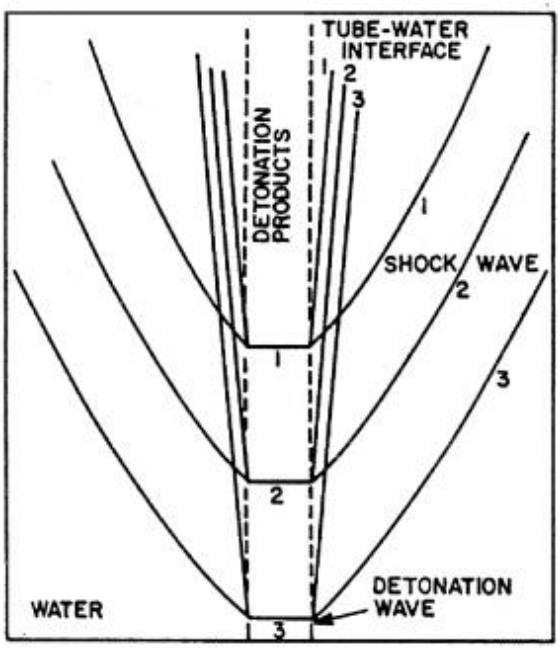

Figure 1.2: Schematic of detonation wave and emanating shockwaves in an aquarium test

One novel idea employs the use of chirped fiber-optic Bragg grating (CFBG) sensors to measure the detonation wave velocity within the explosive (Figure 1.5) [15]. This idea was used by Benterou, et al. [15], to measure detonation velocity of the explosive PBX-9502. Experimental values were between 6.8 and 7.8 km/sec with an expected value of 7.7 km/sec. Initial results were promising, but this method is still in its infancy and needs more testing to be verified.

Another unique idea set forth by Netherwood [16] in 1985 used electrical resistance measured by an oscilloscope to measure detonation velocity. A resistance wire is placed inside of an aluminum tube separated by an insulating thread. As the tube is crushed by the detonation wave, the resistance of the tube/wire assembly changes and the voltage changes can be tracked to extract detonation velocity. A schematic is shown in Figure 1.6 [16]. The results obtained for Detasheet C were within 2% of the nominal published value for the testing density. Detasheet C is a pentaerythritol tetranitrate (PETN) based, rubberized explosive that is manufactured in sheets. While the results may be accurate, the test was limited to testing only Detasheet C and one other explosive. Set-up and equipment need to perform this method are very complicated and time consuming.

Velocity Interferometer System for Any Reflector (VISAR) is another way to determine detonation velocity by measuring particle velocity. A mirror is deposited onto a window normally consisting of PMMA (a transparent thermoplastic). This mirror is then placed against the face of the explosive. A laser is aimed

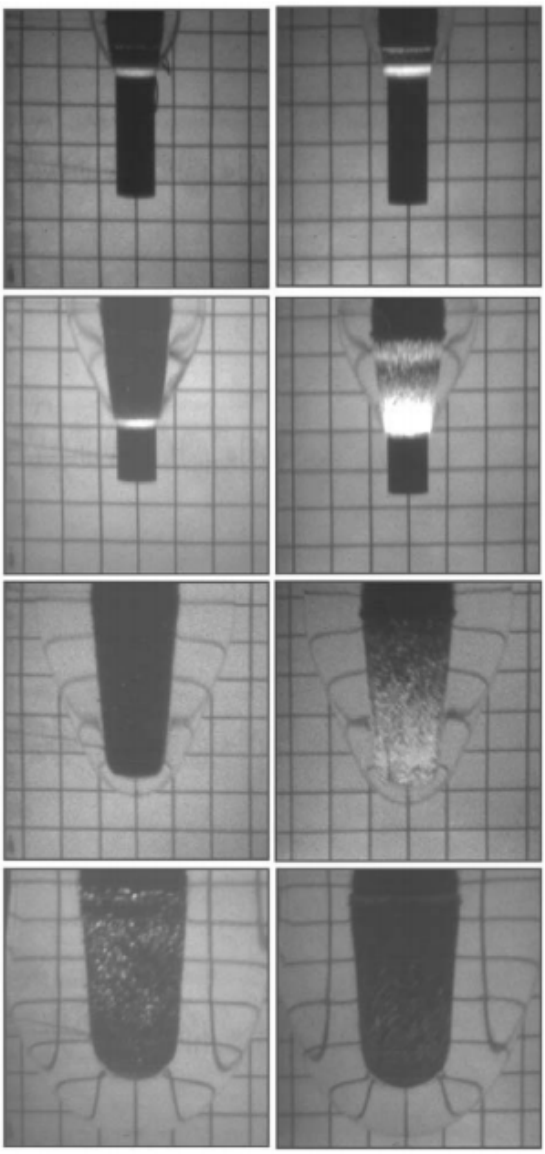

Figure 1.3: Sequential images of an aquarium test

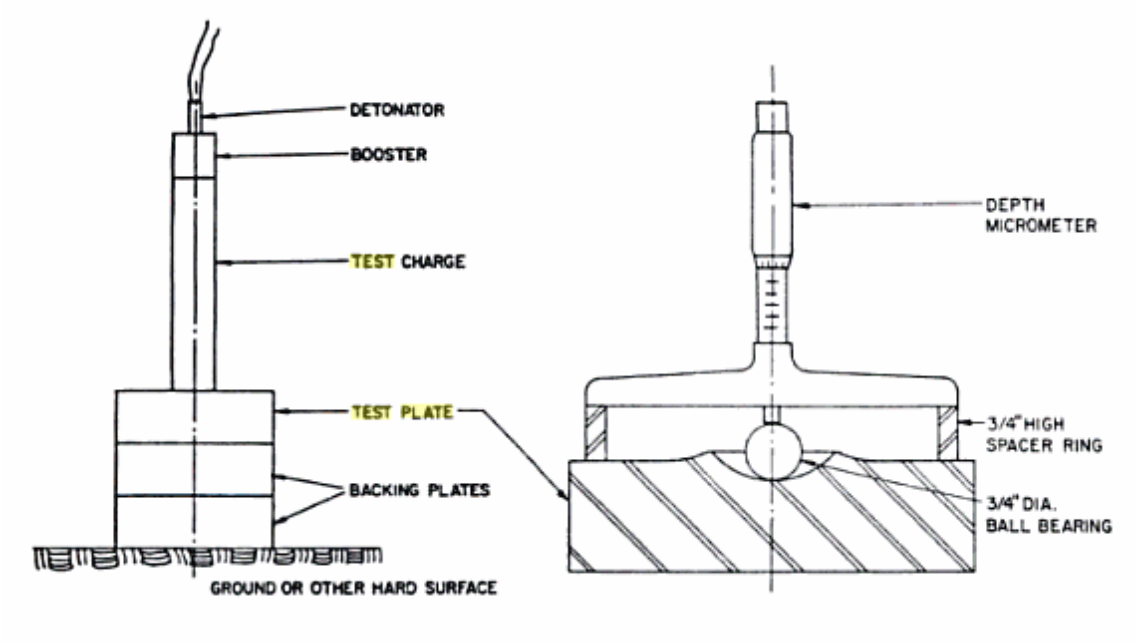

Figure 1.4: Plate dent test configuration

at the mirror and reflected back to the recording equipment. As the detonation reaches the mirror, the mirror moves and the laser light is slightly Doppler shifted which can be detected by the VISAR equipment. The mirror (or interface) velocity can be determined from the Doppler shift. The information is then transformed into an interface versus time waveform.

One such experiment was conducted by Gustavsen, Sheffield and Alcon [17] in which VISAR was used to produce the velocity/time waveform for PBX9501 to resolve reaction zone parameters and establish the ZND point. While this experiment does not attempt to determine detonation velocity per se, it can be determined from the peak particle velocity as long as the peak pressure is also known. By rearranging the Rayleigh line Equation 1.2:

$$P = \rho_0 D u_p \tag{1.2}$$

to solve for D, is Equation 1.3:

$$D = \frac{P}{\rho_0 u_p} \tag{1.3}$$

This method is much too costly and complicated to determine detonation velocity alone, and is usually reserved for determining full detonation parameters for an explosive or material.

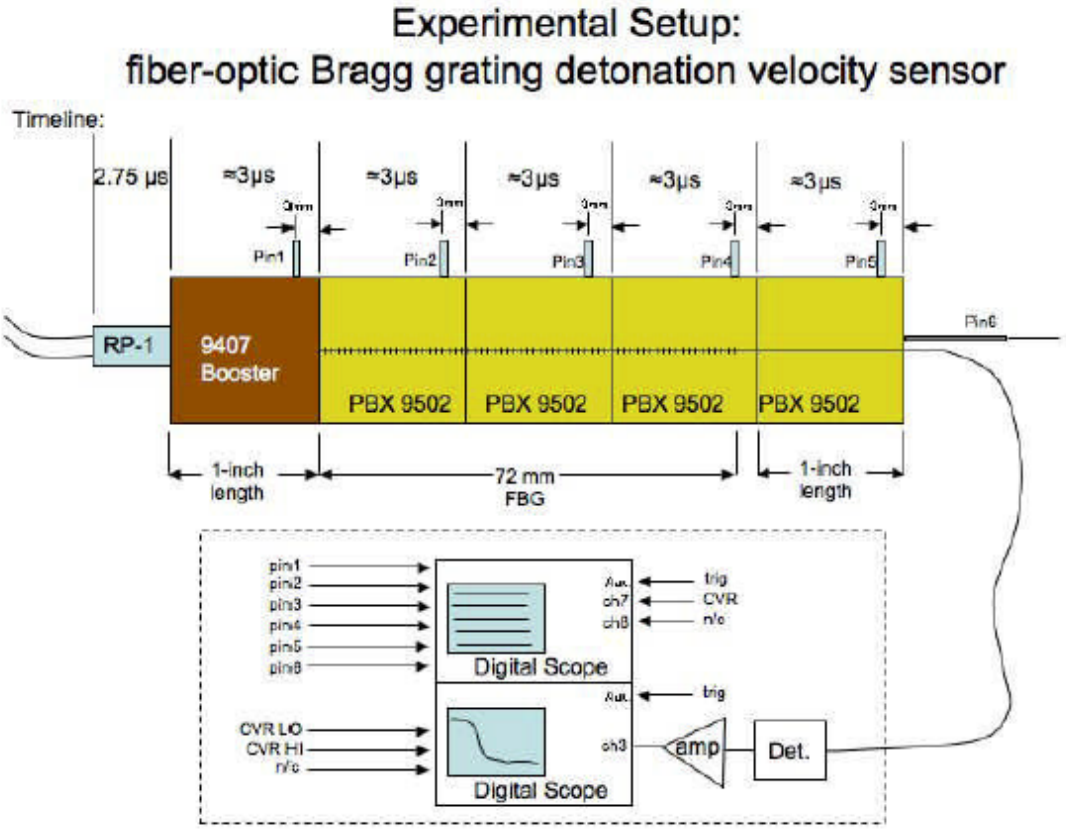

Figure 1.5: FBG detonation velocity sensor set-up

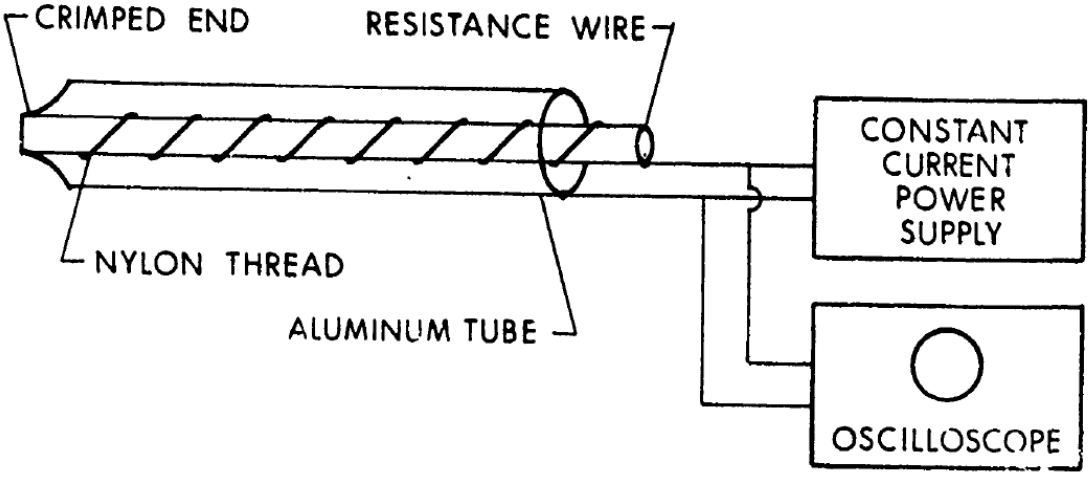

Figure 1.6: Schematic drawing of resistance-wire detonation velocity gage

Photon Doppler Velocimetry (PDV) is a relatively new technique that is quickly replacing VISAR and other interferometry techniques in several applications. According to Holtkamp [18], the application is basically a Michelson interferometer operating at very high speed and is completely enclosed in optical fiber. Instead of one laser, two light sources are combined: one reference light source that has not been Doppler shifted and the other light source is reflected from the moving surface and is affected by a Doppler shift. The signals are recorded with high-speed digitizers, analyzed using Fast Fourier Transform techniques outputting frequency versus time data, and a velocity is found by multiplying the frequency by one-half of the wavelength. The system has advantages over other techniques because it is a small portable system, it can measure a wide scale of velocities, and has equal or better temporal resolution.

Optical methods of measuring detonation velocity are now being tested. A shock wave changes the temperature, pressure, and density of the air as it passes, and therefore changes the refractive index. Snells law indicates that the direction of light rays will be changed due to the difference in refractive indices [19]. Using optical techniques, it is possible to visualize the refraction of the light rays with a camera [6]. If the camera is capable of taking images at a fast rate, it is possible to capture a shock wave on film or digitally.

Most closely related to the research of this study is a technique presented by Biss [4]. He proposed to make laboratory scale measurements of detonation velocity using streak imaging to capture the initial shock wave in air. Streak imaging employs a special camera to measure ultra-fast light phenomena on a temporal scale [20]. Using this ultra-fast imaging (image taken every 6.25 nanoseconds), the initial shock wave was measured out to a distance of 1.2 millimeters. Shock velocity was calculated and linearly extrapolated back to the explosive/air interface.

Rankine-Hugoiniot jump equations are a well know set of equations in explosives engineering [8]. They describe the state of a material after a shock using pre-shock conditions, the physical laws of conservation (mass, momentum, and energy), and experimentally-found material properties. Using these equations, the detonation velocity can be calculated from the shock velocity. The results Biss obtained for RDX (a common military explosive) were within 3% of published values for the densities tested (1.77 g/cc, and 1.63 g/cc) with the exception of detonation pressure for 1.63 g/cc, which was within 10.2%. Biss explains this larger variation by noting the published value for the detonation pressure for RDX at that density was empirically derived and an experimentally measured value was unavailable. This method can be performed on laboratory scale and determines several detonation parameters from a single test, saving time and money over full-scale experiments. However, Biss admits additional testing is necessary to confirm accuracy, and he suggests numerical modeling be performed to confirm that linear approximation is valid.

This study uses a similar approach as Biss to determine detonation velocity from shock velocity, but uses different optical techniques to capture the shock wave on larger scale and at slower time scale. Current lab imaging capabilities

for this study are at a maximum of about 1.5 million frames per second (every 667 nanoseconds). While the Biss study had the ability to acquire 24 images within 1.2 mm from the charge surface, the capabilities for this study is considerably less (approximately seven to ten images within 40 mm of the charge surface). For this reason, the limit of the linear approximation for the shock velocity must initially be validated. The optical techniques to be employed in this study are the schlieren and shadowgraph techniques and are described in the following chapter.

For this study, using these two techniques to visualize the shock, a shock wave velocity profile will be constructed. The shock velocity at the air/explosive interface will be calculated using a linear approximation, and then employing the Rankine-Hugoniot jump equations laid out by Biss [4], the detonation velocity will be determined.

CHAPTER 2

EXPERIMENTAL METHODS

2.1 High-Speed Digital Imaging

Some events of interest take place in such a short time, or objects travel so quickly that conventional cameras are much too slow to film them, such as shock waves. For this reason, the use of more technically advanced cameras is needed. High-speed imaging employs the use of very advanced imaging equipment or high-speed cameras. "Speed" refers to the speed at which the camera can take an image, or the frame rate (frames per second, FPS). The FPS of high-speed imaging is increasing every year, and researchers at Massachusetts Institute of Technology (MIT) have been able to reach 1 trillion frames per second. This is fast enough to even see light traveling through air [21]. Devices that can capture tens of millions of images per second or faster are dubbed "ultra-high-speed". The cost associated with high-speed imaging increases exponentially with the speed of the equipment.

Cameras with imaging speeds of up to 1.5 million frames per second are used for the purpose of this study. Pixel resolution and frame rate are inversely proportional due to memory limitations. To utilize the highest frame rate, the field of view must be small with a resolution of only 128 x 8 pixels. Tests are conducted at a range of distances from the charge center, but of main concern for this study is the imaging of the shock wave in the near-field (one to five charge diameters) and very-near-field (within one charge diameter). Far-field is said to be over 5 charge diameters away, but all of these terms are loosely used and do not have established values.

Exposure times range from 0.294 μs to 2 μs depending on the frame rate and light source used. Light sources that emit more light lend themselves to shorter exposure times. Since lighting is critical for high speed imaging, the aperture is normally fully open for all lenses used throughout testing. Short exposure times (along with high frame rate) are important so that the images of the shock wave's leading edge are as crisp and well-defined. Exposure times that are too slow will produce blurry or smeared images resulting in a larger margin of error during image processing. Self-illumination can lead to over-exposed images when trying to capture images within the first few microseconds of the explosion. Neutral density filters are employed to help reduce the amount of light captured by the camera.

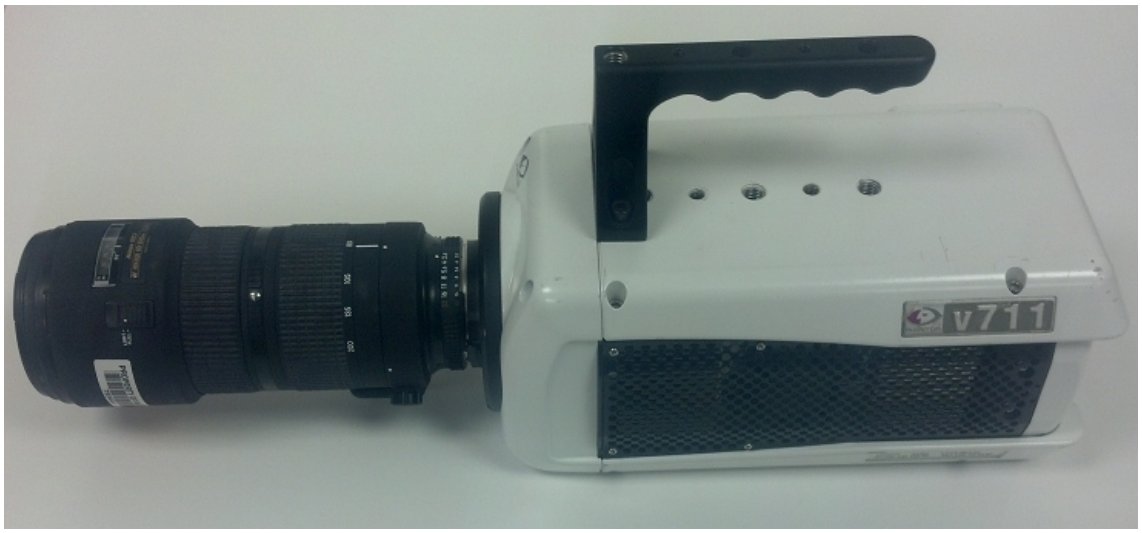

Figure 2.1: Phantom V711 camera

A calibration object is needed to determine the number of pixels in given distance. The calibration object is placed in the field of view and snapshot is taken using the high-speed camera. A calibration object that fills as much of the field of view as possible is preferable to decrease error. A new calibration image is needed whenever any parameters of the test are changed.

2.1.1 Equipment

The cameras used for this research are the Phantom V711 by Vision Research and the Photron FASTCAM SA-X2. Both cameras have black-and-white capabilities only, as color pictures are of no consequence when imaging shock waves and therefore have no impact on this study. The Phantom V711 has an internal 8 GB RAM and a maximum resolution of 1200 x 800. At this resolution, a speed of 7530 frames per second (fps) can be achieved with a record time of about 1.5 seconds. At a resolution of 128 x 8, the maximum speed that can be attained is 1,511,111 fps with a record time of 2.75 seconds. While the resolution can be set as low as 32 x 8 pixels, the maximum frame rate and record time are the same as the 128 x 8 resolution. Figure 2.1 shows the Phantom V711 camera with no lens attached.

The Photron SA-X2 also has an internal 8 GB RAM with a maximum resolution of 1024 x 1024 pixels with frame rates from 1000 fps to 12,500 fps and corresponding record times of 5.45 seconds and 0.43 seconds. The minimum resolution is 128 x 8 pixels with a frame rate of about 1 million fps and a record time of 5.58 seconds.

Record times of two seconds or more are sufficient for the cameras to be triggered manually and still capture the event with sufficient settings for pre-trigger and post-trigger recording. Recording time can be extended with the

addition of RAM, but this will not increase the recording speed. The Phantom camera is preferred for this testing as it has the higher frame rate at the lower resolutions. The high frame rate helps lower uncertainty by providing a more crisp and defined shock front in the image (i.e. less smearing of the shock) which makes pixel selection during image processing easier. The Phantom also has an event-based trigger built into the camera that makes finding the small changes much easier when sorting through hundreds of thousands or even millions of frames.

The lens used for testing is a Nikon ED Nikkor 80-200 mm lens. Single images were taken with a Nikon D5100 digital camera with a Nikon DX AF-S Nikkor 18-55 mm lens. The software used to view the recorded images for the Photron is PFV version 338 (x64) Photron FASTCAM Viewer, and the Phantom uses the Phantom PCC software version 2.14b.

The light source for the majority of testing is an arc lamp that uses a xenon bulb that has an output of 1000 watts, and is manufactured by Newport Corporation, Model 66921, with lamp part number 6271. The power supply is also by Newport Corportation, Model 69920. Other tests use an ordinary automobile headlight lamp Model 9005 Silverstar Ultra by Sylvania with a BK Precision DC Regulated Power Supply, Model 1627A, with variable output from 0 - 30 volts DC at 3 amps.

Tests are set up on Newport optical tables with aluminum optical rails secured to the table with bolts. The required lenses and all other equipment needed, including the camera, are secured to the rail with optical rail mounts. The rail mounts are adjustable in height and can be fixed where needed at any point along the rail. The rail helps to ensure the equipment is aligned along one axis. Collimating lenses were used to create parallel light rays in the test area. The lenses are 12.7 cm in diameter and have a focal length of 70 cm.

2.2 Imaging Techniques

Shock waves are nearly invisible and travel at high velocities making it difficult if not impossible to be seen with the naked eye. A shock wave increases the temperature, pressure and density of the medium it passes through and changes the refractive index. This change in properties causes the light rays to bend in the region of the shock front, towards the region of higher density [22]. On camera, the front of the shock wave will look like a dark line followed by a region of intensified light. The dark region is where the light should have appeared had it not been bent by the difference in refractive indices. Instead, the light is bent inward, towards the origin of the shock wave. This bent light now intensifies the light in the region just behind the shock front at an angle determined by the intensity of the shock wave. Two unique optical techniques are employed to capture the shock wave on camera and are described below.

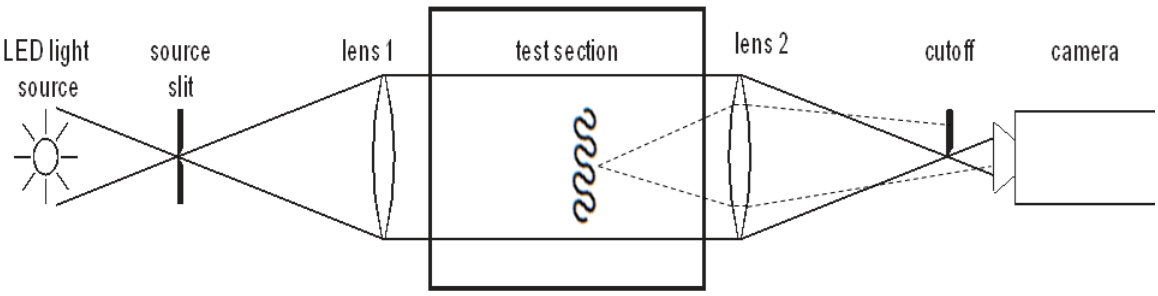

Figure 2.2: Schematic of a typical lens schlieren system

2.2.1 Schlieren Technique

Schliere are visible streaks in a transparent medium due to a change in density and therefore refractive index within the medium. Schliere (German for streak) were first seen in 1665 by Robert Hooke. Through a lens, Hooke observed the non-homogeneous properties in air created by the turbulence of warm air rising from a lighted candle, using a second candle in the background as the light source [6]. This was the crudest of set-ups, and more sophisticated techniques are used today and in the collection of data for this research.

Schlieren imaging first requires a light source to illuminate the schlieren object from somewhere beyond the object in relation to the camera. The light passes through a slit or small hole to create a point light source and to block any stray light rays from other sources. A collimating lens is used to capture light from the point light source and create parallel light rays. A second lens collects the light and is focuses onto a cutoff, or knife blade [6]. The area between the two lenses becomes the test area. The disturbance, or schlieren object, is placed in the test area where any change in the density of the medium (air) will refract light. The cutoff is needed to block some of the bent light created by the schlieren object. This will produce the light and dark regions as seen by a camera placed near the cutoff. The camera is focused on the object in the test area. As seen in Figure 2.2, some of the refracted light (bottom dashed line) will pass by the knife edge and into the camera lens. Some of the refracted light (top dashed line) will be blocked by the knife edge and subsequently be darker on the image in a camera.

A picture of a candle using the schlieren technique is shown in Figure 2.3. The right side of the flame is dark since the light from that side is refracted into the knife edge, while the left side is bright from light being refracted into the lens.

Figures 2.4 and 2.5 show the typical set-up used during the course of this study.

Figure 2.3: Photo of candle using schlieren imaging technique

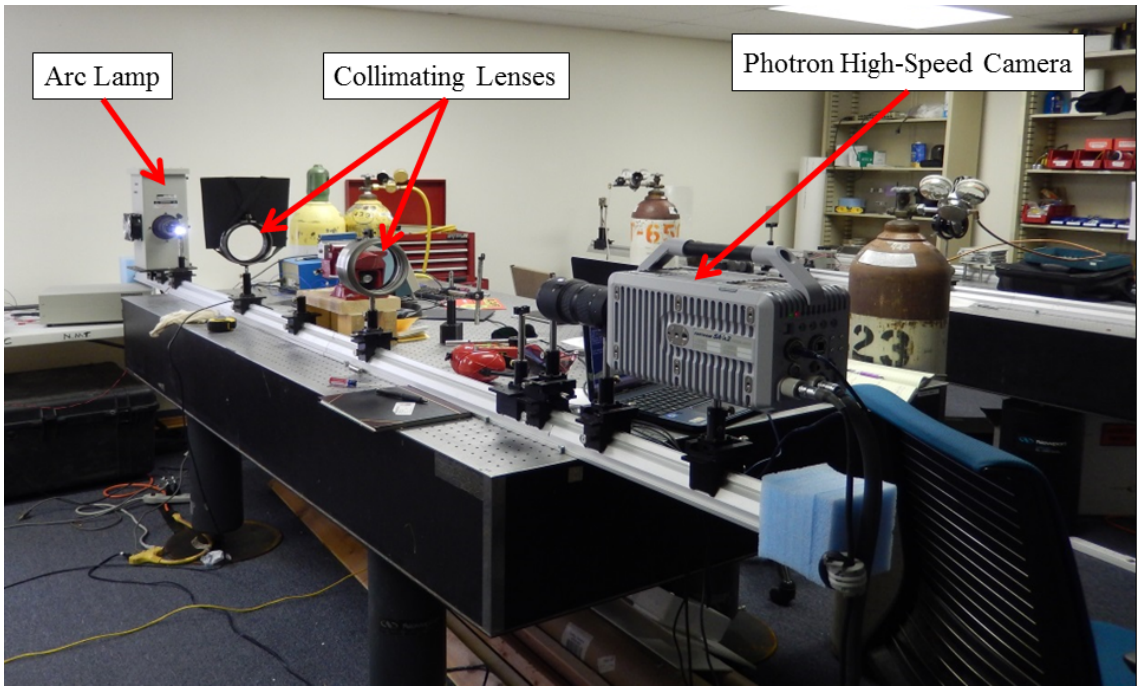

Figure 2.4: Lab set-up

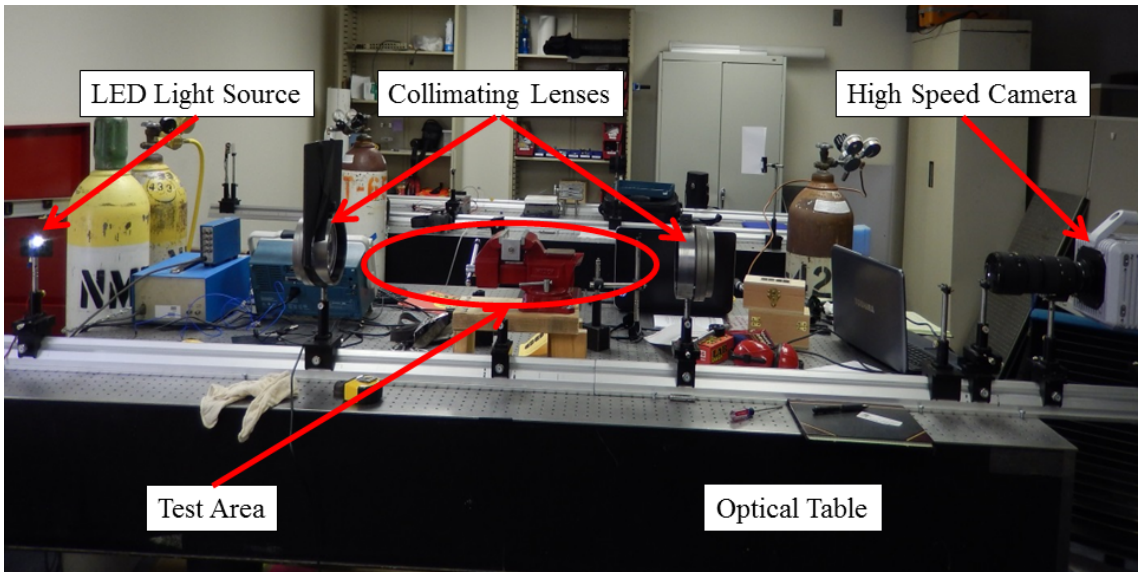

Figure 2.5: Lab set-up

2.2.2 Shadowgraph Technique

The shadowgraph technique can be much easier to use in that its simplest form only requires a light source, the schlieren object, and a flat, reflective surface [6]. The set-up used for experiments in this study is slightly more complicated and is shown in Figure 2.6. Light is focused from the light source to a point on a mirrored rod attached to the lens of the camera. A UV (ultraviolet) filter can be used at the light source to eliminate most of the UV radiation emitted by the bulb. The mirrored rod is cut at a 45-degree angle so that the light from the source is reflected 90 degrees towards a retro-reflective screen. The mirrored rod on the lens is small compared to the aperture of the camera so that it does not interfere with the image returning to the camera from the screen. A retro-reflective surface is one that reflects light back in the same direction from which it came [23]. The schlieren object is in the path of the reflected light (from the mirror) and the shadow of the refracted light from the object is projected onto the screen. The camera is focused onto the screen and records the shadow imagery. As seen from the geometry of the shadowgraph set-up, the image is not in one-to-one correspondence between the object and the shadow. Geometric correction is needed to provide true image measurements. The angle epsilon, ϵ, in Figure 2.6 is the angle at which the light is bent and is dependent on the refraction index of the schlieren object, S.

Shadowgraphy lends itself to be used on a much larger scale than the schlieren technique [23][24]. Retro-reflective screens come in various sizes and several retro-reflective screens may be joined together to provide a very large background. Since the traditional schlieren technique employs lenses and sometimes mirrors, the scale on which it can be implemented is limited by the size of

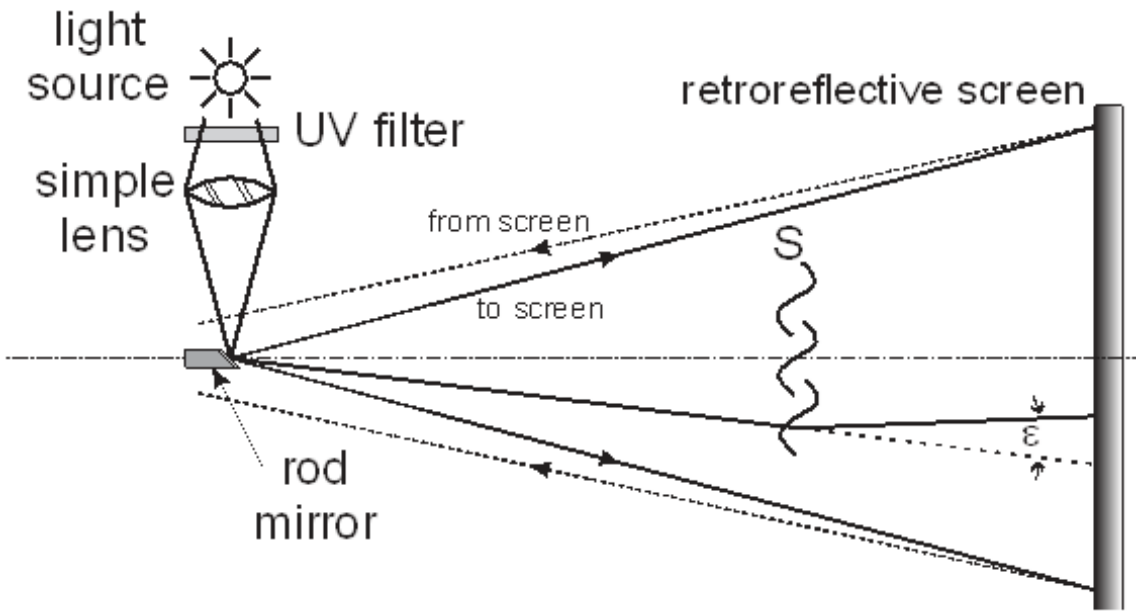

Figure 2.6: Schematic of a typical shadowgraph system

the optical equipment.

Both techniques were utilized during this research, but the schlieren imaging technique is preferred for this study as it presents the imagery on a one-to-one scale without the need for correction. It lends itself well to the scale on which this research was conducted and provides the necessary sensitivity to visualize the shock. The images are also better suited for quantitative analysis.

2.3 Testing of Primers

Primers made for shotgun shells are tested to compare test results with the known properties for the explosive compound contained within the primers. The primers used are the Remington 209 Premier STS shotgun shell primers. A firing mechanism specifically designed to fire shotgun primers is used to fire the primers and is shown in Figure 2.7.

The tip of the primer is flush with the end of the insert that holds the primer as to capture the initial burst from the primers initiation hole. Figures 2.8 and 2.9 show the aluminum block that holds the firing mechanism in place a close up of the end of the firing mechanism held in a vise. The initiation hole of the primer can clearly be seen in Figure 2.9.

Figure 2.10 shows the mechanism disassembled, the aluminum block that holds the mechanism, a primer, a package of primers, and an extraction tool used to screw and unscrew the insert that holds the primer in the end of the firing

Figure 2.7: Shotgun shell primer firing mechanism

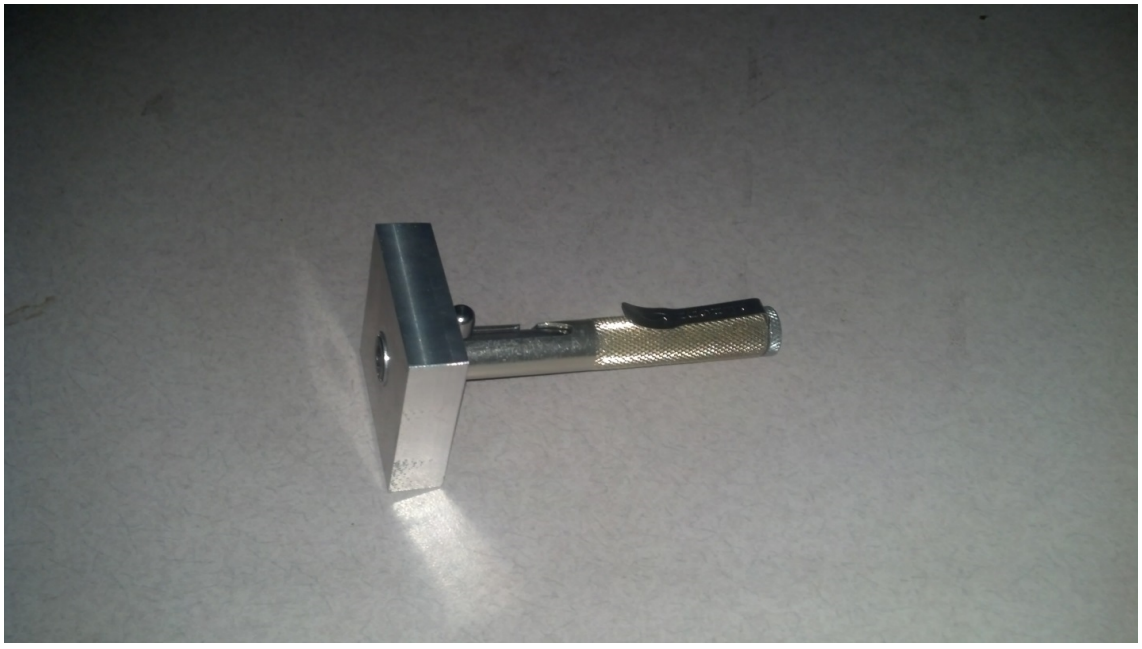

Figure 2.8: Firing mechanism and holding block

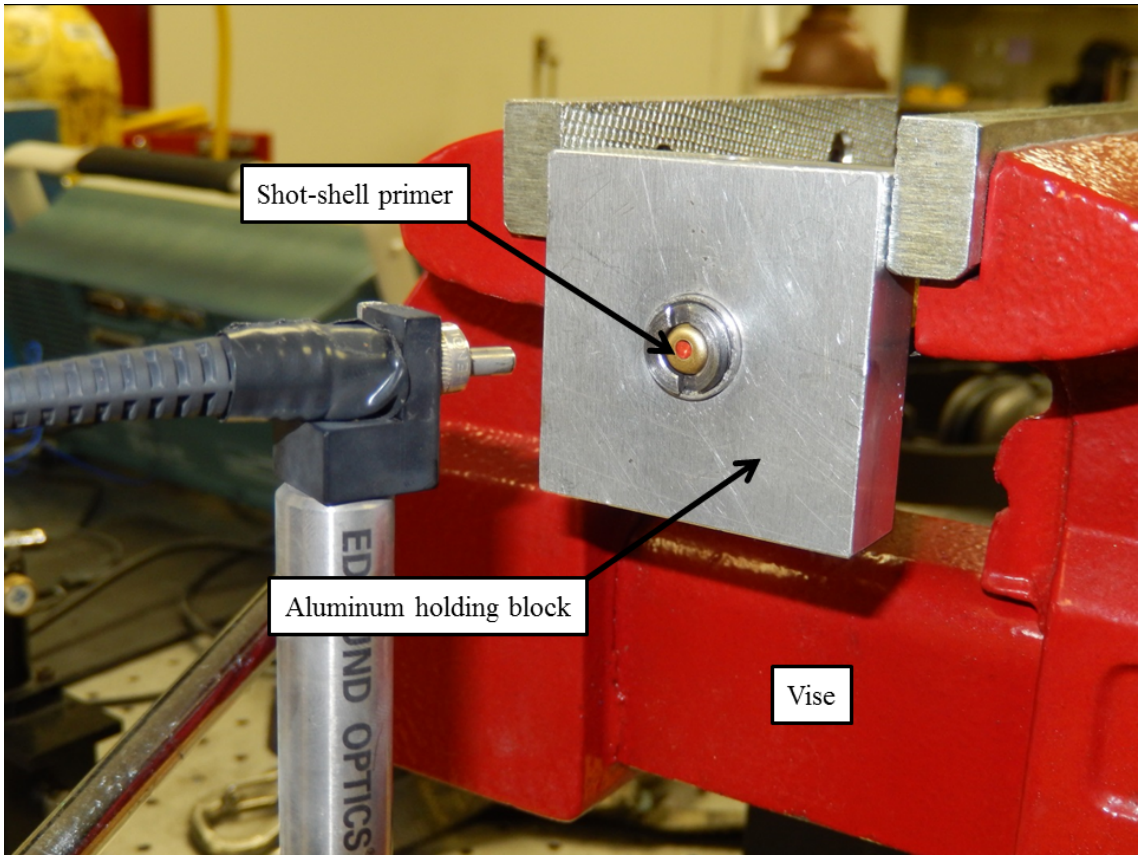

Figure 2.9: Block and firing mechanism held by vise

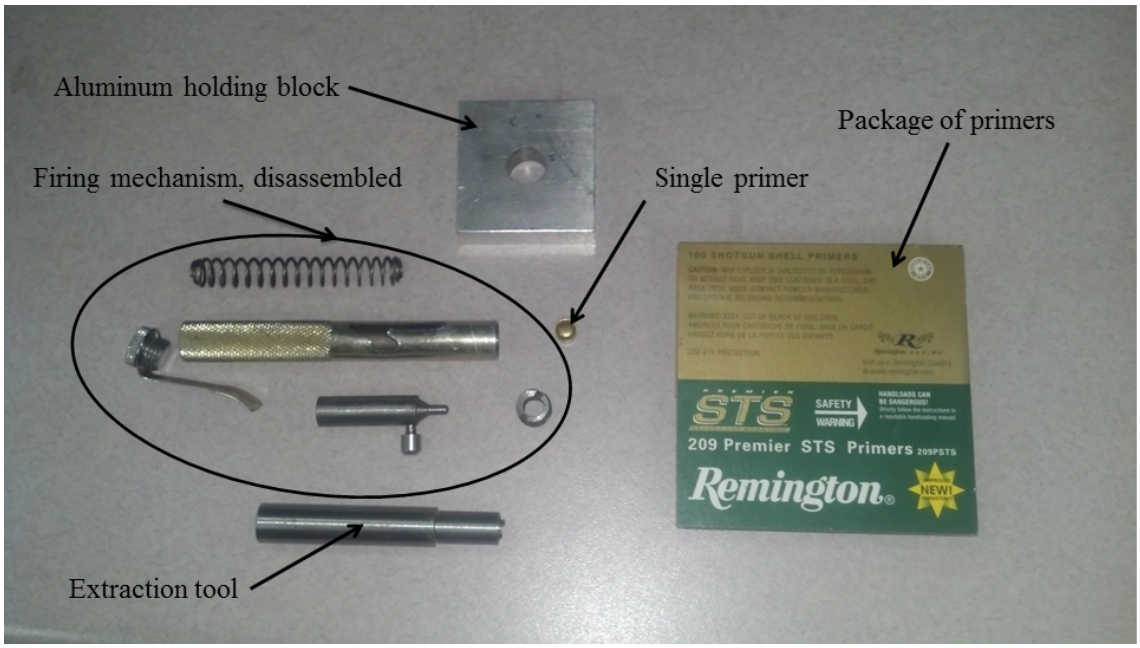

Figure 2.10: View of the firing mechanism disassembled, the holding block, a primer, a primer extraction tool, and a package of shot-shell primers

mechanism. The primers are fired and the resulting shock wave is captured using the schlieren imaging technique.

2.4 Testing of NONEL®

NONEL® (NON-ELectric) is a shock tube initiation system used to detonate explosives. It is a hollow tube that has the inside coated with an explosive compound. The explosive propagates along the length of the tube at approximately 2000 m/sec and initiates a detonator attached to the end of the tube. The explosion in the tube is of such low energy that the tube is largely undamaged after firing.

The shock tube used in testing was NONEL® Lead Line and the explosive coating is a mixture of HMX and fine aluminum powder. The set-up for testing NONEL® is shown in Figure 2.11 with a close-up of the tip of the shock tube.

No detonators are attached to the end of the shock tube for testing, so that the shock exiting the end of the tube is examined. The end of the tube is held in place using the optical equipment seen in the photo. The starting end of the shock tube can be initiated several different ways. A high-voltage electric firing set is used for the current set of tests. The detonation velocity is obtained from the shock velocity and compared to the published detonation velocity for HMX.

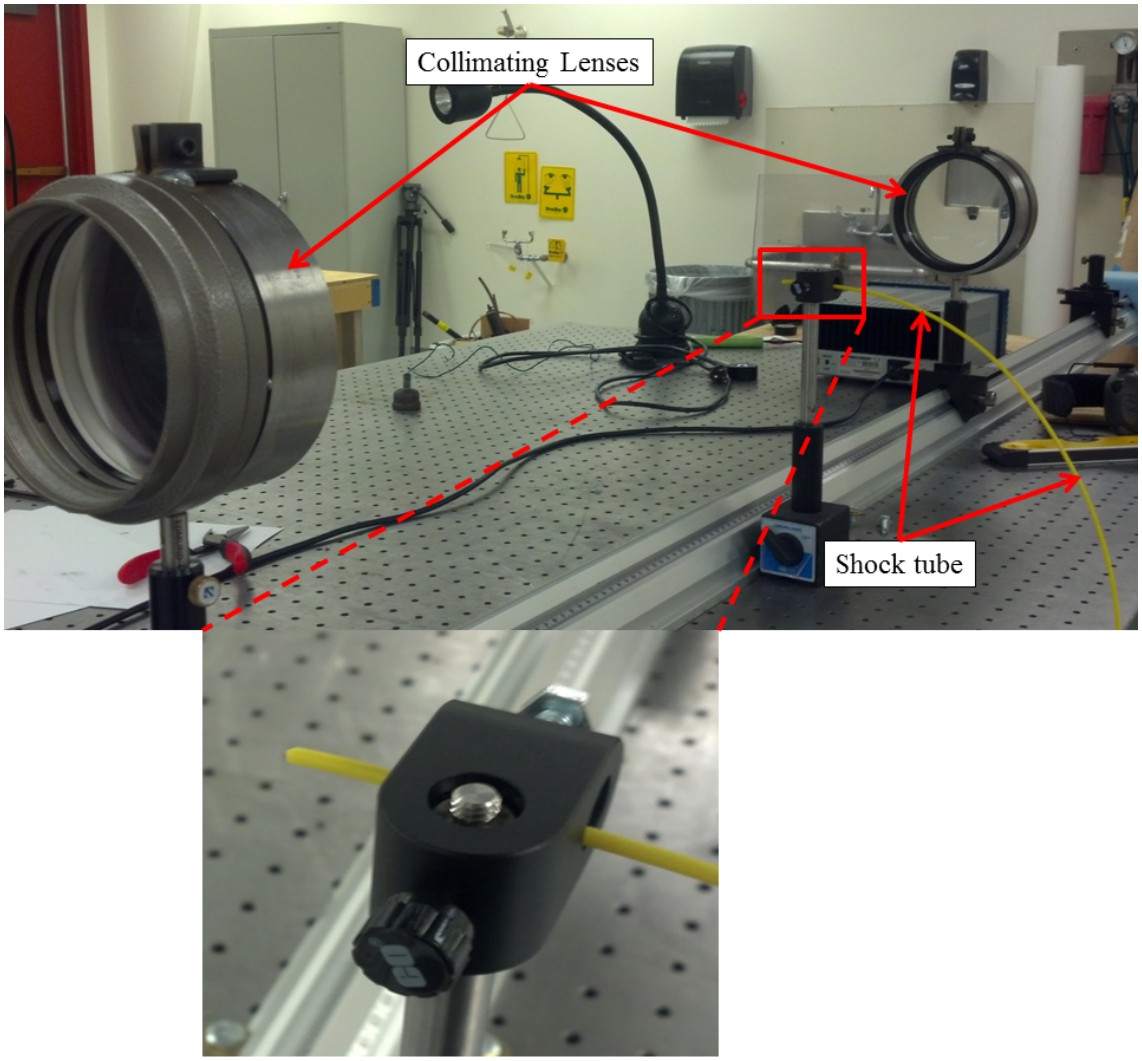

Figure 2.11: Set-up of shock tube test and close-up of NONEL®

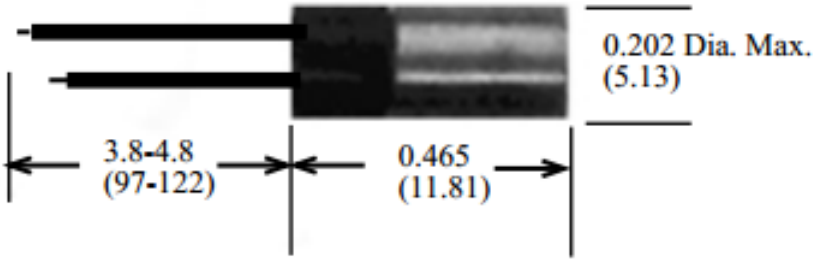

Figure 2.12: RP-2 detonator with dimensions in inches (mm)

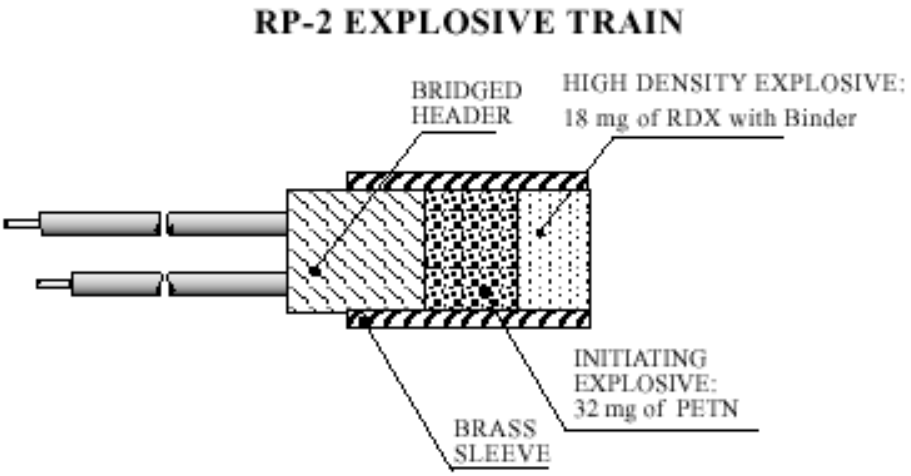

Figure 2.13: Schematic of RP-2 detonator

The length of the shock tube used varied in length for each test, but was on the order of a few meters. A steady propagation wave is needed to get accurate results. It is shown by Obed (et al.) that a steady propagation wave is achieved after only 225 mm [25].

2.5 Testing of RP-2 Detonators

RP-2 EBW (exploding bridge-wire) detonators are small explosive devices manufactured by Teledyne RISI, Inc. and used to initiate other explosives. Figure 2.13 shows the dimensions of the detonator while Figure 2.12 shows the components of the detonator [26].

A small metal wire within the detonator explodes when a high enough current is applied within a small amount of time. The exploding wire then initiates the explosive surrounding it (PETN) which in turn initiates the high density explosive (RDX).

Tests are run using the schlieren technique to capture the shock wave created from the explosion, and the calculated detonation velocity is compared to published values of the explosives.

2.6 Method of calculating detonation velocity

All of the images taken were processed using a MATLAB code [5] that tracks the shock in successive frames. The program then returns pertinent data to an Excel file and two graphs are generated; one of shock radius versus time and another of shock Mach number versus radius. From the graphs, the initial shock velocity can be determined.

The detonation velocity, D, of an energetic material can be found knowing only the shock velocity, U, at the interface of the explosive reaction products and the surrounding air. The shock velocity is only one of five parameters that define a shock wave. The four others are particle velocity u, density ρ (or specific volume ν), pressure P, and specific internal energy e. Five variables necessitates five equations to solve the system. Three equations are conservation equations (mass, momentum, and energy) and known as the Rankine-Hugoniot jump equations (Equations 2.1, 2.2, and 2.3). These equations describe the state of the material before and after the shock.

$$\frac{\rho_1}{\rho_0} = \frac{U - u_0}{U - u_1} = \frac{\nu_0}{\nu_1} \tag{2.1}$$

$$P_1 - P_0 = \rho_0(u_1 - u_0)(U - u_0) \tag{2.2}$$

$$e_1 - e_0 = \frac{P_1 u_1 - P_0 u_0}{\rho_0(U - u_0)} - \frac{1}{2}(u_1^2 - u_0^2) \tag{2.3}$$

The subscripts 0 and 1 denote the pre-shocked and post-shocked state, respectively. Two more equations are necessary to define the shock. One desired equation would relate specific internal energy such that it is a function of pressure and specific volume (much like the ideal gas law):

$$e = f(P, \nu) \tag{2.4}$$

Then this could be combined with the energy jump equation (Equation 2.3) to eliminate the specific energy term:

$$P = f(\nu) \tag{2.5}$$

This leaves two equations in four variables (P, U, u, and ν). Of the six possible relationships between any two of the four variables, three have been found to be most useful. These are the U-u, P-u, and P-ν relationships.

The U-u relationship was experimentally found to be a linear equation for most materials:

$$U = C_0 + su \tag{2.6}$$

The constants C_0 and s are specific to a material and found empirically. Equation 2.6 combined with the momentum equation (Equation 2.2) yields the P-ν relationship, Equation 2.8, and a simple rearrangement of Equation 2.6 returns Equation 2.7. Further study by Biss [4] combined with the work of Cooper [8] produces the rest of the equations (Equations 2.9, 2.10, and 2.11) needed to reach the objective of detonation velocity determination.

$$u = \frac{U - C_0}{s} \tag{2.7}$$

$$P = \rho_{air} C_0 u + \rho_{air} s u^2 \tag{2.8}$$

$$\rho_{CJ} = 1.386 \rho_e^{0.96} \tag{2.9}$$

$$u_{CJ} = exp \frac{ln\left(\frac{\frac{Pu^{8.71}}{235\frac{\rho_{CJ}\rho_e}{\rho_{CJ}-\rho_e}}}{}\right)}{10.71} \tag{2.10}$$

$$D = \frac{u_{CJ}\rho_{CJ}}{\rho_{CJ} - \rho_e} \tag{2.11}$$

Combining the information gathered from the high-speed images and the above equations, the detonation velocity can be determined. This is then compared to published values of detonation velocity for accuracy and will be discussed in the next chapter.

Some assumptions must be made in order to use the method described above. First of all, the expansion of the gaseous products is assumed to be a one-dimensional flow. While the flow approximately follows a semi-spherical pattern from the initiation point, we can assume 1-D flow along the axial centerline of the cylindrical explosive. Also, the explosives are assumed to be ideal, that is, the reaction zone is infinitely small. This is called the Chapman- Jouguet (CJ) model.

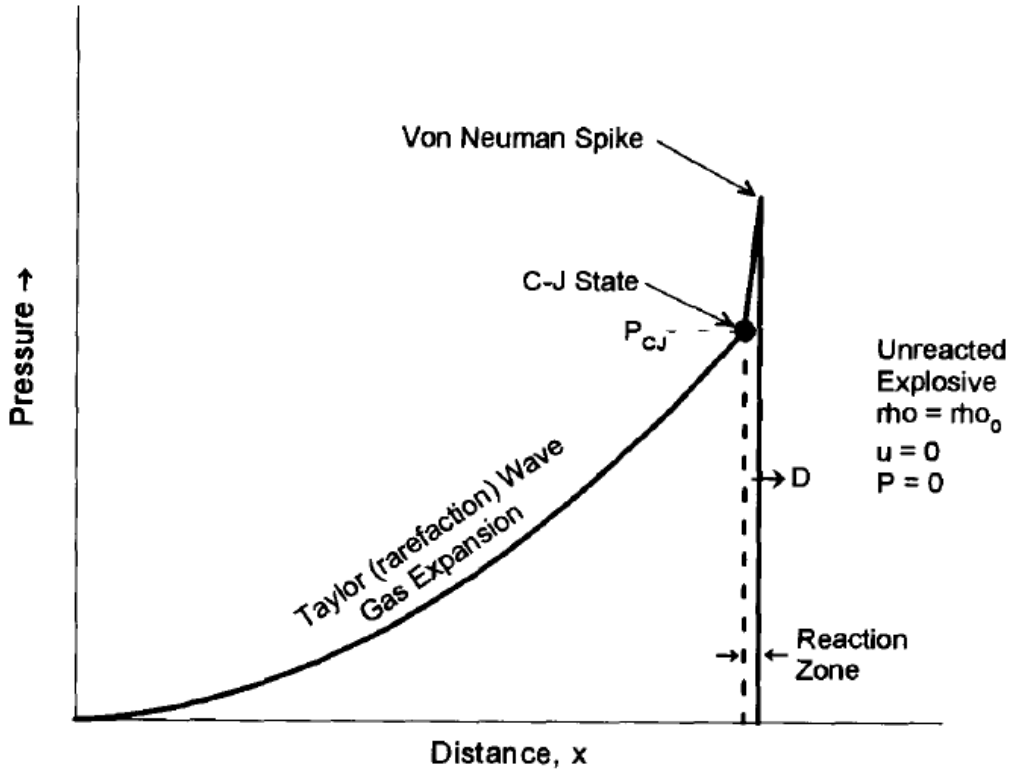

Figure 2.14: Pressure/distance graph of detonation wave

Figure 2.14 [8] depicts the pressure vs. distance diagram of the Zeldovich, Von Neumann, and Deering (ZND) model, which is the same as the CJ model but includes the reaction zone. It shows a 1-D detonation wave traveling from left to right. The reaction zone is the area directly behind the leading detonation wave and is of finite thickness, the end of which is depicted by the dashed line. The Von Neumann spike is the theoretical maximum pressure of the detonation and occurs at the detonation front. If the reaction zone was infinitely small, the maximum pressure would be at the CJ state, denoted by P_{CJ} on the figure. The CJ point denotes the steady-state detonation point. The detonation velocity calculated from the above equations is determined at the CJ state.

The images for the RP-2 tests were analyzed manually and the data was processed using Microsoft Excel. The reason for this is that the images for the RP-2 tests did not contain a well-defined shock front that is required to use the MATLAB code. These images are shown in the following chapter.

CHAPTER 3

RESULTS AND DISCUSSON

Tests were performed with shotgun shell primers, NONEL® shock tube, and RP-2 detonators. Each test item was initiated and the resulting shock wave was captured with a high-speed camera. The shock wave velocity was analyzed and a detonation velocity corresponding to the explosive compound in each item was found. The desire was that this experimentally found detonation velocity would be in congruence with published values for detonation velocity.

3.1 Shotgun Shell Primers

Shotgun shell primers were used as a small scale explosive to validate the detonation velocity determination technique. The primers used in testing were Remington 209 Premier STS Primers. Several compounds are present in the primer case, but the main explosive ingredient is lead styphnate according to the material safety data sheet (MSDS) obtained from Remington Arms [27]. For example, tetrazene is added to increase the sensitivity to percussion [28]. The presence of other compounds introduced a challenge in finding a suitable published detonation velocity to compare to experimental results. As lead styphnate is the main explosive compound, the information obtained for that compound was used for comparison. According to the Lawrence Livermore National Laboratory (LLNL) Explosives Handbook, the detonation velocity for lead styphnate is 5.2 km/s at a density of 2.9 g/cc [29]. The actual loading density for the lead styphnate used in the primers is unknown, so the value given above is the one used to compare with the results from testing.

Many primers were fired to get a statistically significant data set. As tests progressed, the field of view narrowed and the frame rate increased to try to get data at the limits of the camera used. Testing was done to come as close as possible to reproducing the results obtained by Biss [4], but using the equipment available. It should be noted here that the streak camera Biss used was running at the equivalent of 80 million frames per second, while the current camera used had an upper limit of just over 1.5 million frames per second. Most tests were run at a significantly smaller frame rate. Higher frame rates led to very low pixel differences between frames, while the highest frame rate resulted in a shock wave movement of only two or three pixels per frame when the zoom on the camera

lens was set at 80 mm for the focal length. Since the error used was $\pm$ 1 pixel, the error of the shock velocity at any one point was subject to large error, but the overall shape of the curves (radius/time and Mach number/radius) was consistent throughout testing. The camera lens was set at its maximum focal length of 200 mm to help remedy the problem of small pixel jumps in sequential frames. This improved the pixel difference to 7 or 8 pixels between frames.

3.1.1 Far-Field Testing

Tests were run at a large field of view to get a shock velocity profile for the widest view possible, limited by the size of the collimating lenses which had a diameter of 127 mm. Figures 3.1 and 3.2 show five tests where the field of view was 122 mm and frame rates varied from 30,000 to 260,000 frames per second. Figure 3.1 shows the fairly linear nature of the shock radius versus time for these frame rates and distances. Figure 3.2 show that the peak shock velocity varies from about Mach 1.5 to Mach 2.3. The frame rates used during these tests were not high enough to capture the shock near the interface of the air and explosive nor the peak shock velocity which are the items of interest. Therefore, the frame rate must be increased and the field of view needs to be narrowed to the region near the air-explosive interface. From Figure 3.2 it is seen that after approximately 30 mm, the shock wave has degraded to nearly a sound wave. These tests show that the most critical information is located within a 30 mm radius of the face of the primer. The curve fit equation used for radius/time graphs in this study use the form:

$$R = A + Ba_0t + Cln(1 + a_0t) + D\sqrt{ln(1 + a_0t)} \tag{3.1}$$

and was proposed by Dewey [30]. R is the radius, a_0 is the speed of sound in the medium (air), and t is time. The coefficients A, B, C, and D are unique to a given explosive and found by using a least-squares regression program written in MATLAB by Hargather [5]. The curve fit equation for the Mach number/radius graphs is found by taking the derivative of Equation 3.1 with respect to time and dividing by the speed of sound, a_0.

3.1.2 Near-Field Testing

Many tests were run to obtain a statistical average data set and several of these tests are plotted in Figures 3.3 and 3.4. Figure 3.3 shows tests run with the camera lens set at 80 mm focal length and Figure 3.4 shows tests imaged with the camera lens set at 200 mm focal length. Both figures show that the shock radius versus time is fairly linear, and therefore the shock velocity is nearly constant. In order to get the best possible result, the peak shock velocity must be resolved, which is expected to be at the explosive/air interface. Figures 3.5 and 3.6 show the Mach number versus radius from the charge. The peak value for the shock

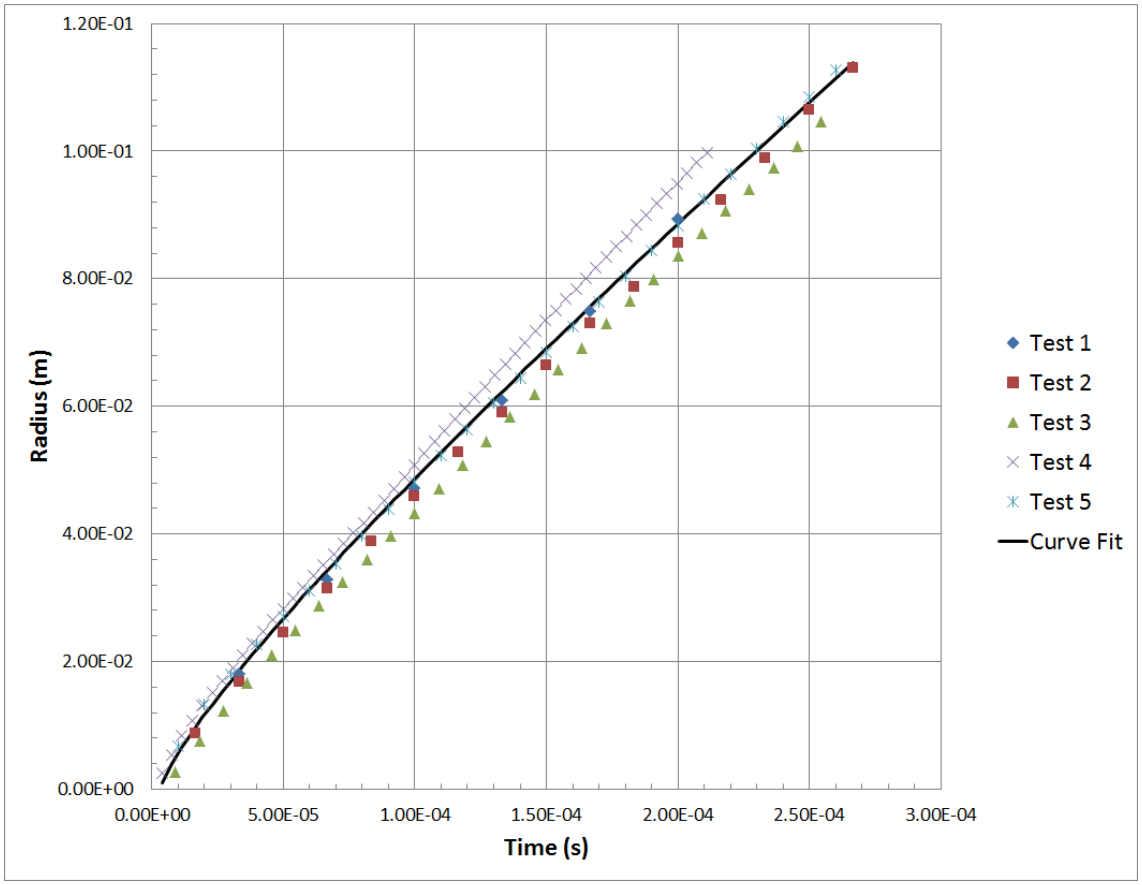

Figure 3.1: Far-field primer data - radius/time graph

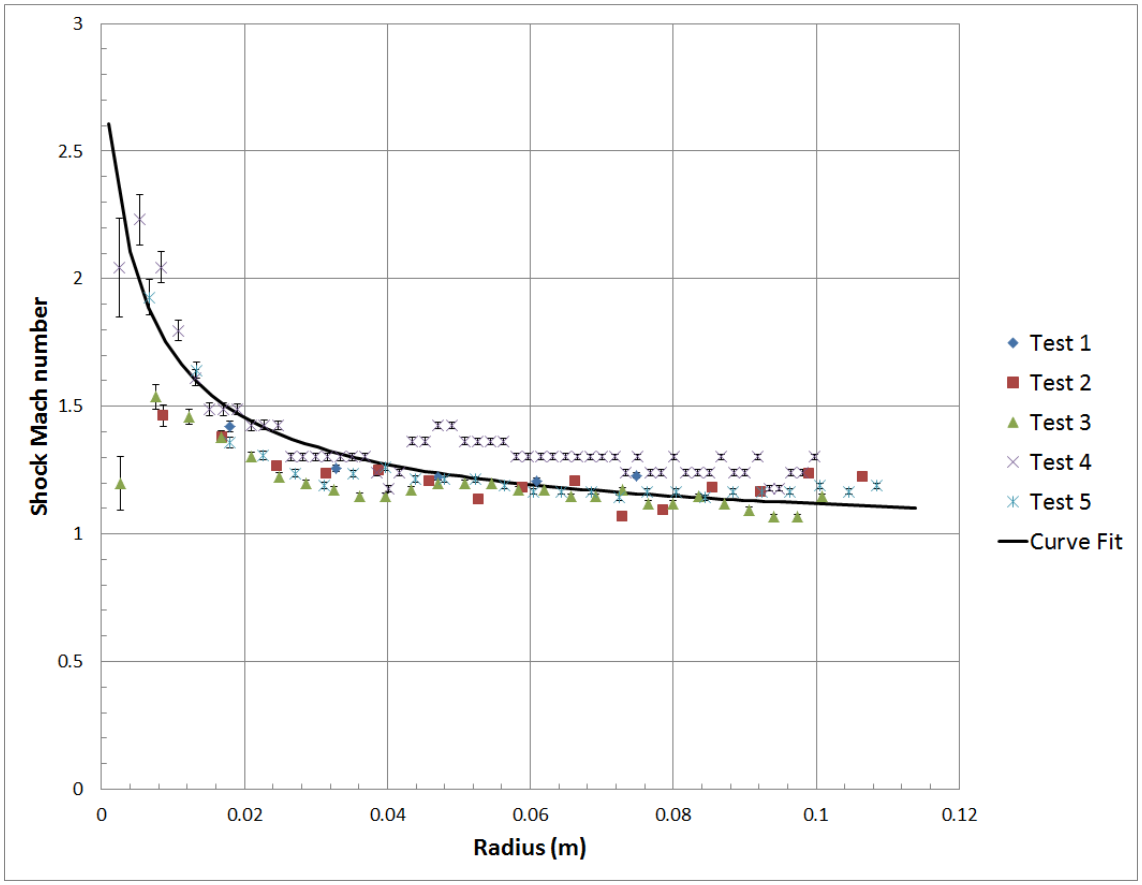

Figure 3.2: Far-field primer data - Mach/radius graph

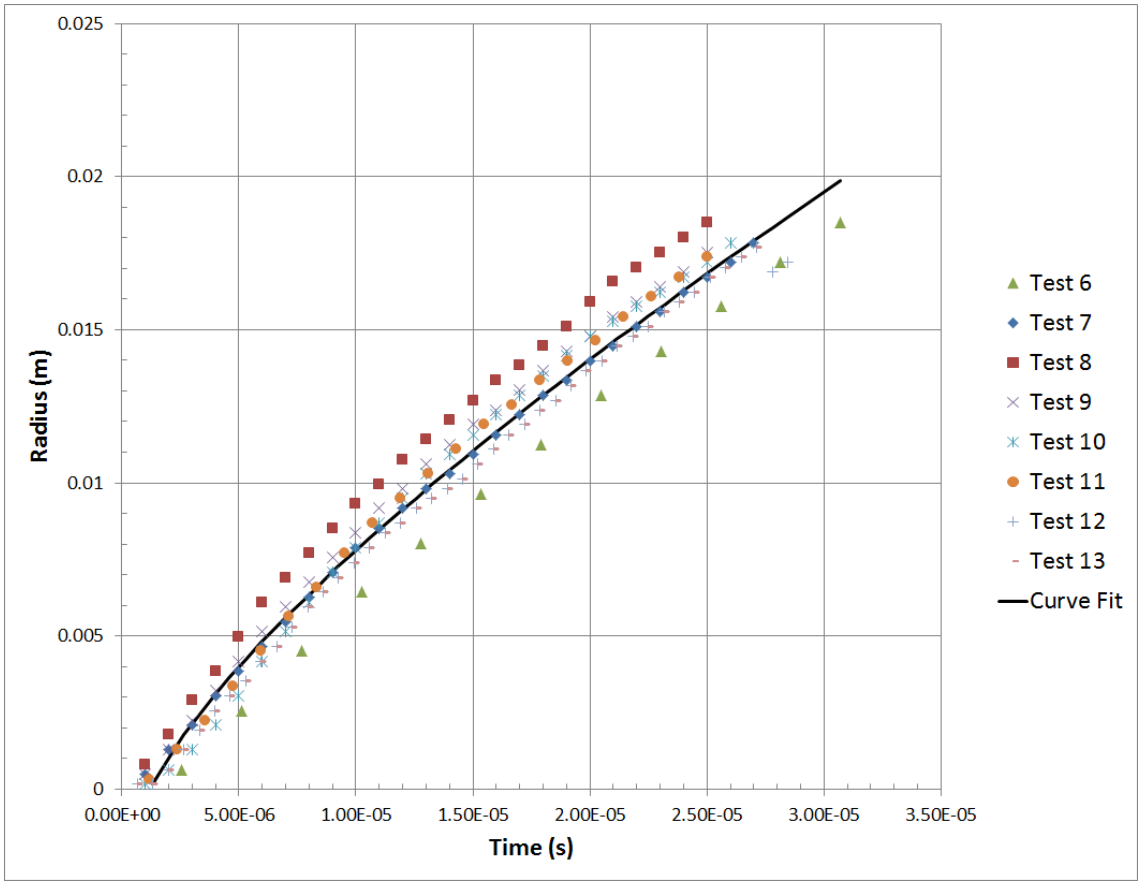

Figure 3.3: Near-field primer data - radius/time graph, 80mm zoom

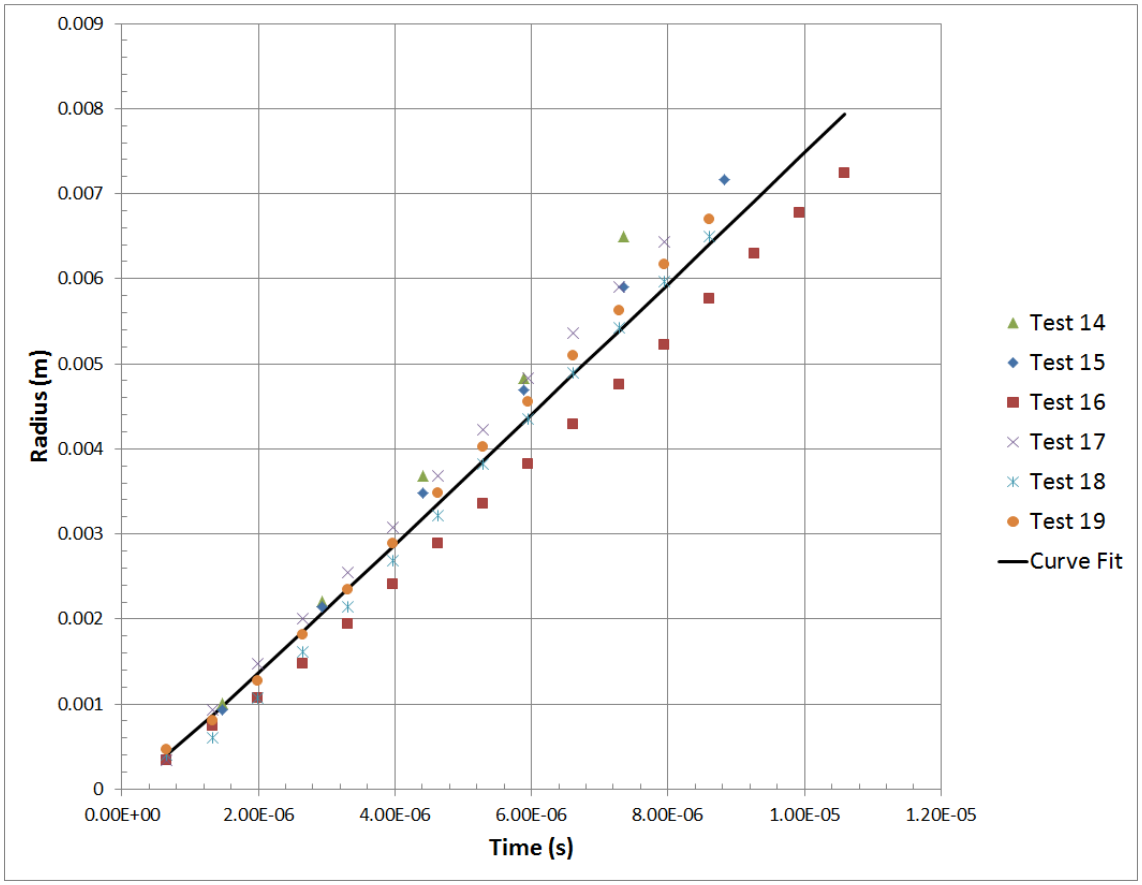

Figure 3.4: Near-field primer data - radius/time graph, 200 mm zoom

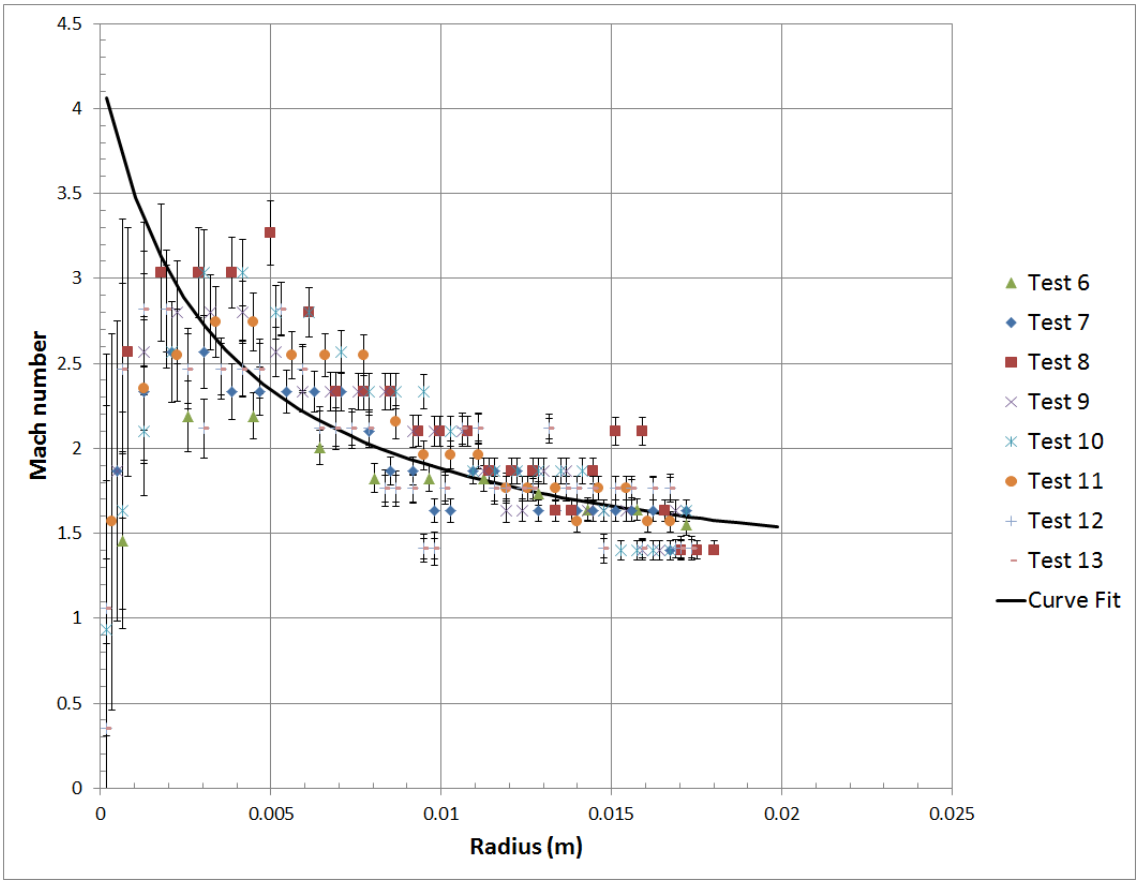

Figure 3.5: Near-field primer data - Mach number/radius, 80 mm zoom

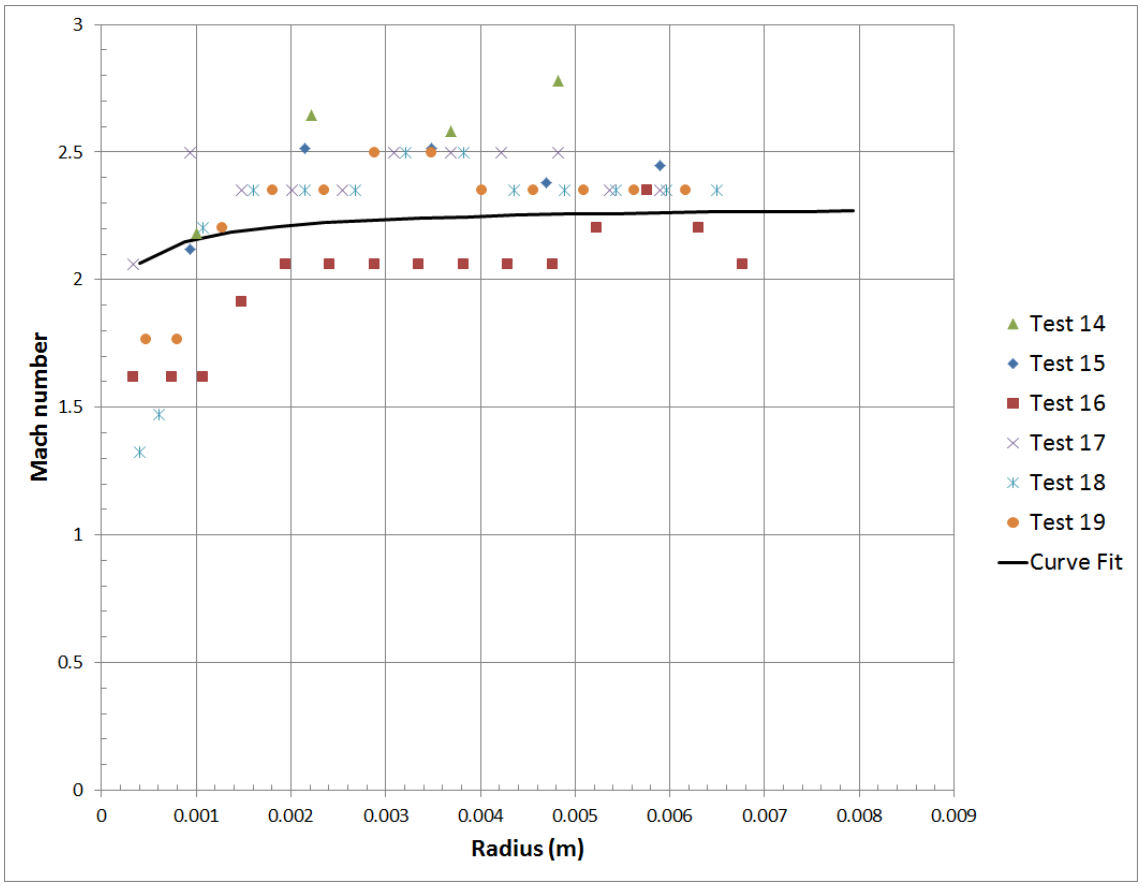

Figure 3.6: Near-field primer data - Mach number/radius, 200 mm zoom

velocity varies from about M 2.0 to M 3.3 (0.68 to 1.12 km/s). One method to check results is to work the calculations used by Biss [4] in reverse order. This will result in an expected shock velocity from the published detonation velocity. Using the published detonation velocity of 5.2 km/s, the peak shock velocity at the interface is expected to be 5.6 km/s. This is much higher than the results obtained for any primer test.

The highest shock velocity obtained during testing (1.12 km/s) only returns a detonation velocity of 0.87 km/s compared to the published value is 5.2 km/s. This is off by almost a magnitude of order and has a wide variation. The peak value on the curve fit line in Figure 3.5 is about Mach 4.1; if this is used to calculate the detonation velocity, the result is 1.13 km/s. Test results for shock velocity and detonation velocity are only 12% to 20% of the expected value, while the curve fit velocity is about 22% of the expected value.

Figure 3.6 shows the Mach number versus radius for the tests run with the camera lens zoomed in to its maximum of 200 mm. Rising shock velocity can be seen within the first few millimeters of the face (discussed below); then, the velocity is almost constant, and the curve fit line is nearly constant at Mach 2.25. None of the tests run with the camera lens zoomed in reached a peak velocity of that in the previous tests run with the lens zoomed out. This is unexpected, as tests run with higher zoom have a higher spatial pixel resolution which would lead to a more accurate account of the shock front velocity. Peak shock velocity was widely varied and inconsistent over the entire set of data, and is supported by this Figure 3.6.

A troubling observation of the Mach/radius curves is that the shock velocity increases for the first few millimeters from the primer face. This is not typical behavior of ideal explosives. The peak shock velocity normally is at the explosive/air interface and the jump is instantaneous. Possible reasons for the discrepancy in expected shock velocity, variation in shock velocity, and the shape of the Mach/radius curves are:

- There are other ingredients in the primers that may be affecting the performance.
- There is a physical barrier (a paper foil) that the explosion must breach before propagating outward. Also, the shock must emerge from a flash hole in the end of the primer. This hole is constricting and the shock does not always emerge symmetrically.
- The amount of lead styphnate may be so small that a steady state detonation is not reached. This may be by design. Gun manufacturers may only want (and probably only need) deflagration in order to ignite the powder inside the shot shell.
- The primer detonation is not an ideal detonation, and the shock is being fueled by the expanding gases and continuing detonation/deflagration of the reactants for the first few microseconds.

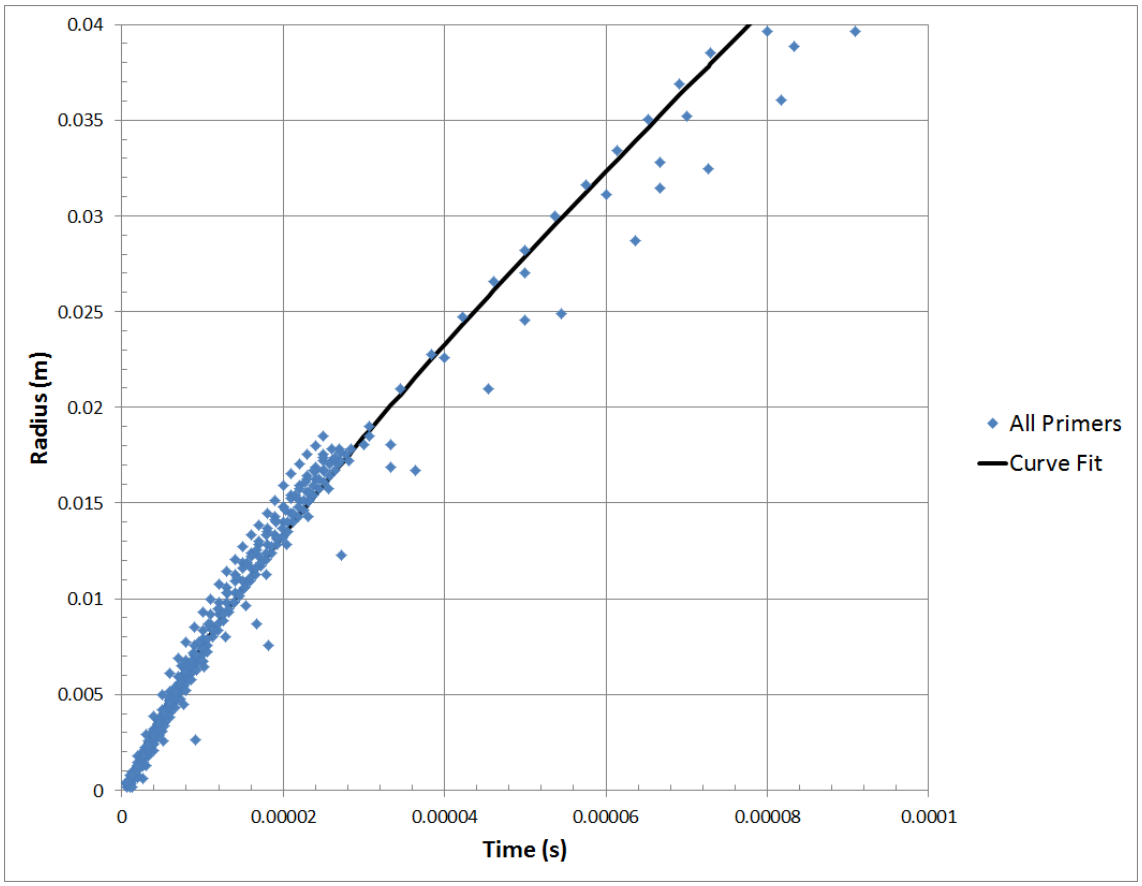

Figure 3.7: Graph of all primer data

- There are several inconsistencies in the manufacturing of the primers.

Figure 3.7 show all primer data plotted on one graph with a corresponding curve fit.

Streak imaging is another tool that can help analyze high-speed images. These streak images were not taken with a streak camera; they are merely a temporal account of one horizontal row of pixels in the image of the high-speed camera used for the tests. Figure 3.8 is a streak image of one of the primer tests and shows what normally should happen in an explosive event. The horizontal spacing between the markers (the white pixels) is larger at the beginning of the event, which is at the top of the figure. The horizontal spacing decreases as the shock front moves further away from the initiation point. This indicates that the shock front velocity is decreasing as well. The vertical spacing is the same for each marker, as this is the time between sequential frames.

Streak cameras have the capability to record at ultra-high speeds and the image is recorded on film, so resolution is essentially infinite. The use of streak cameras would eliminate two problems that arise with the use of digital high-

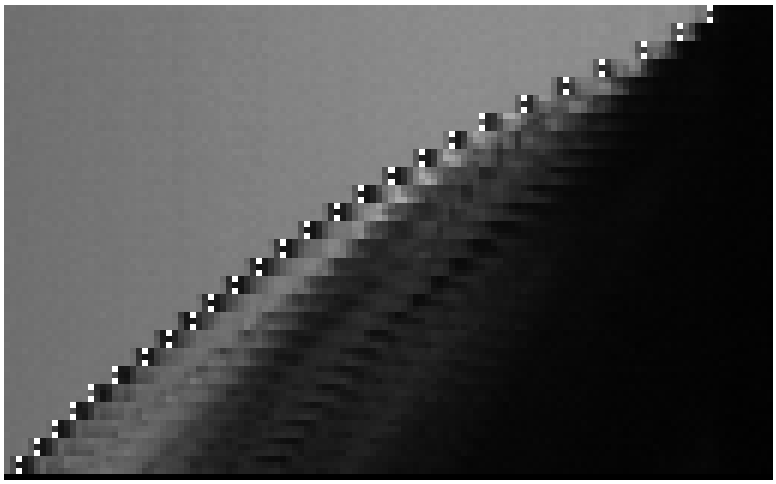

Figure 3.8: Streak image of a normal primer test

speed cameras: (1) the ultra-fast imaging would almost eliminate the problem of determining the exact initiation time. Digital high-speed cameras are limited to about one microsecond between frames, in which the event begins between frames zero and one; the time when the event started between the frames is not known. Since a streak camera has a much higher temporal resolution (at least three orders of magnitude better), the time the even started can be more exact; (2) pixelation would be eliminated by the use of film and the spatial resolution of the shock front could be better determined. The use of film is also one drawback of using a streak camera: the film must be developed whereas a digital camera has images available immediately. Other disadvantages are that the streak cameras are more expensive and the setup and use is more difficult.

The main purpose of this research is to provide a relatively inexpensive, portable, easy-to-use system to set up in a laboratory setting for the determination of detonation velocity. The use of fairly common, digital high-speed cameras would facilitate that goal. Streak cameras cost approximately $250,000 and up while the high-speed cameras used here cost less than $100,000.

Figure 3.9 is a streak image of an atypical test. The spacing at the beginning is slightly closer together than the spacing later on in the event. This indicates that the shock is moving faster than in the beginning. This demonstrates that this explosive event is far from ideal.

3.2 NONEL® Testing

The shock tube known as NONEL was also tested using this method. The reported propagation velocity of the shock wave in the NONEL tube is 2100 $\pm$ 300 m/s. It should be stressed that this is a propagation value, not the detonation velocity. The explosive content of the shock tube is approximately 90% HMX and

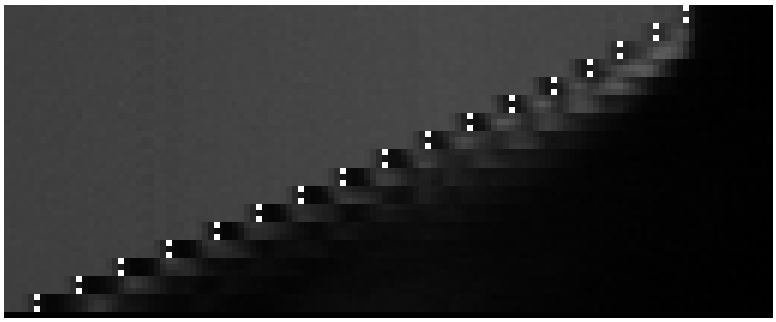

Figure 3.9: Streak image of an atypical primer test

10% aluminum powder. Detonation velocities for HMX and several HMX mixtures were found, but none matched the mixture in the shock tube. The assumed density of the explosive powder inside the tube was taken to be 1.66 g/cc and have a detonation velocity of 7.77 km/s. Most of the values found for detonation velocity are assumed to be the solid crystalline density of HMX or a solid casting of the HMX mixtures. The mixture inside the shock tube is a powder so the lowest density found in publications was used as the comparison value.

Figure 3.10 shows the radius/time graph of the tests run with a larger field of view while Figure 3.11 shows the radius/time graph of the tests run at a higher frame rate and smaller field of view. All NONEL® test data is fairly consistent over the span of tests as shown in Figures 3.10 and 3.11. All tests have the lens of the camera set to the 200 mm focal length with the exception of Test 1. As mentioned before, the most pertinent data is within the first few millimeters of the face of the tube, so the zoomed in lens gives us the best set of images to extract the data.

Figures 3.12 and 3.13 show the Mach number/radius graphs. Similar to the primer tests, the most significant data to be gathered is within 20 to 30 millimeters of the end of the tube. Peak shock values were in the range of approximately Mach 2 to 4. Using the highest peak value of Mach 3.9, the detonation velocity was calculated to be just over 1 km/s. This is half of the published propagation velocity of 2.1 km/s.

Similar to the primer tests, some NONEL® tests showed an increase in the shock velocity within the first few millimeters from the end of the tube. This is thought to be error in selecting the correct pixel location of the shock front due to the extremely bright fireball at the beginning few frames and not due to reasons given for the primers.

Figure 3.14 shows a graph of all NONEL® data taken along with a corresponding curve fit.

Several problems were encountered with testing the shock tube. Foremost, the light production of exploding HMX is so great that the initial shock wave could not be seen clearly near the tip of the tube. The addition of aluminum to the HMX only exacerbates this problem. The flash of light can be seen in the

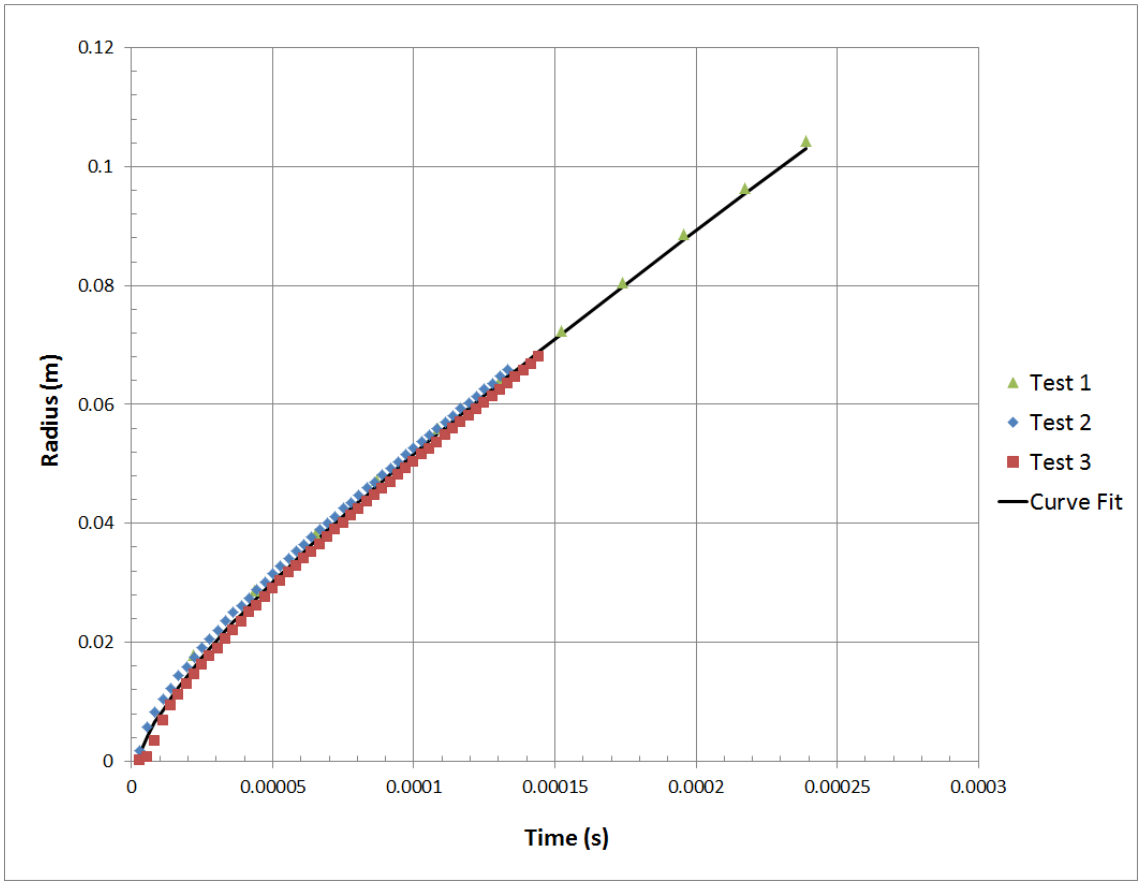

Figure 3.10: Far-field NONEL® tests, radius/time graph

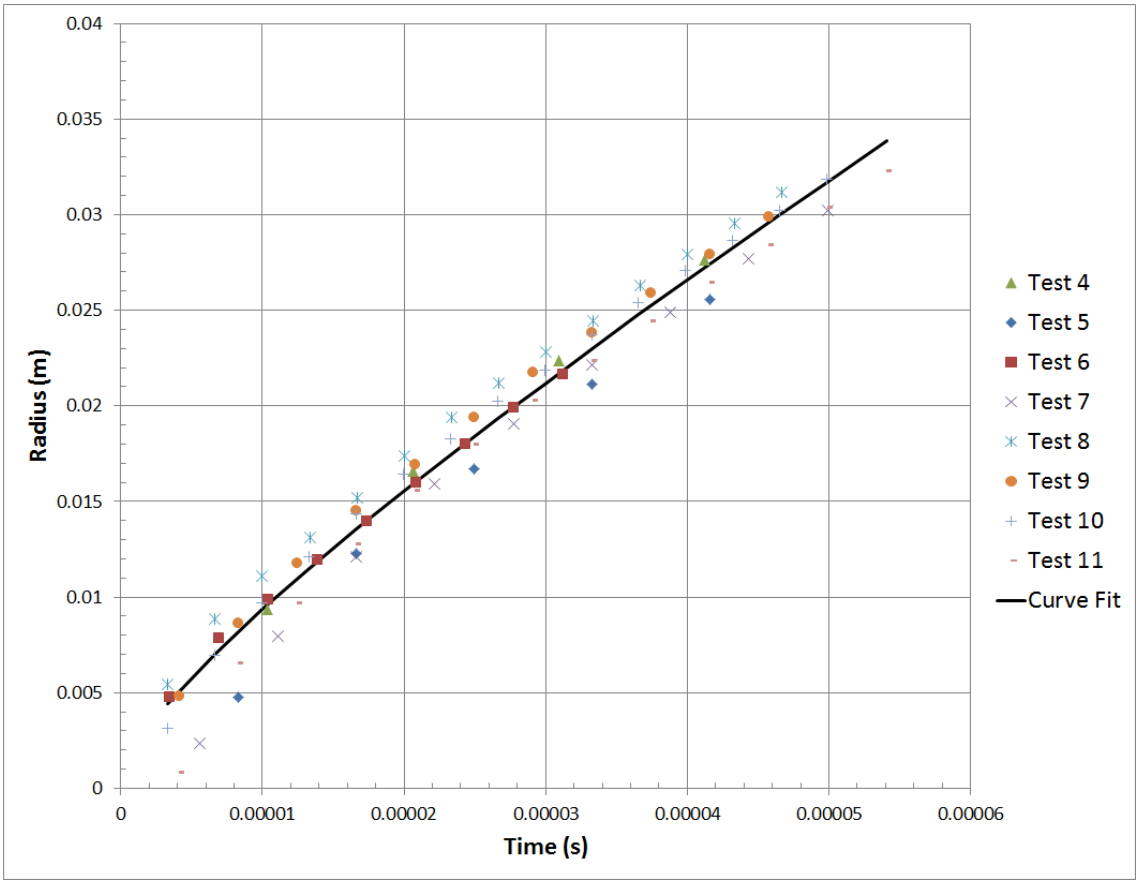

Figure 3.11: Near-field NONEL® tests, radius/time graph

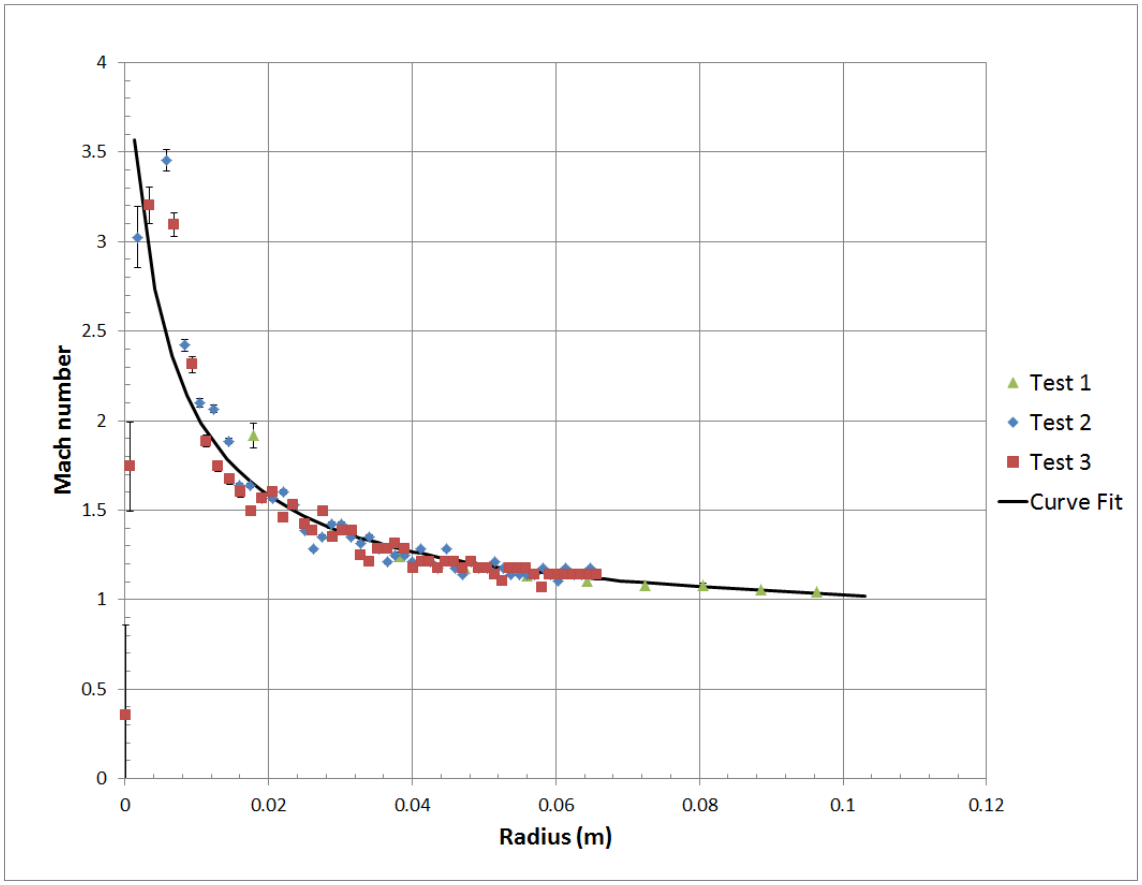

Figure 3.12: Far-field NONEL® tests, Mach number/radius graph

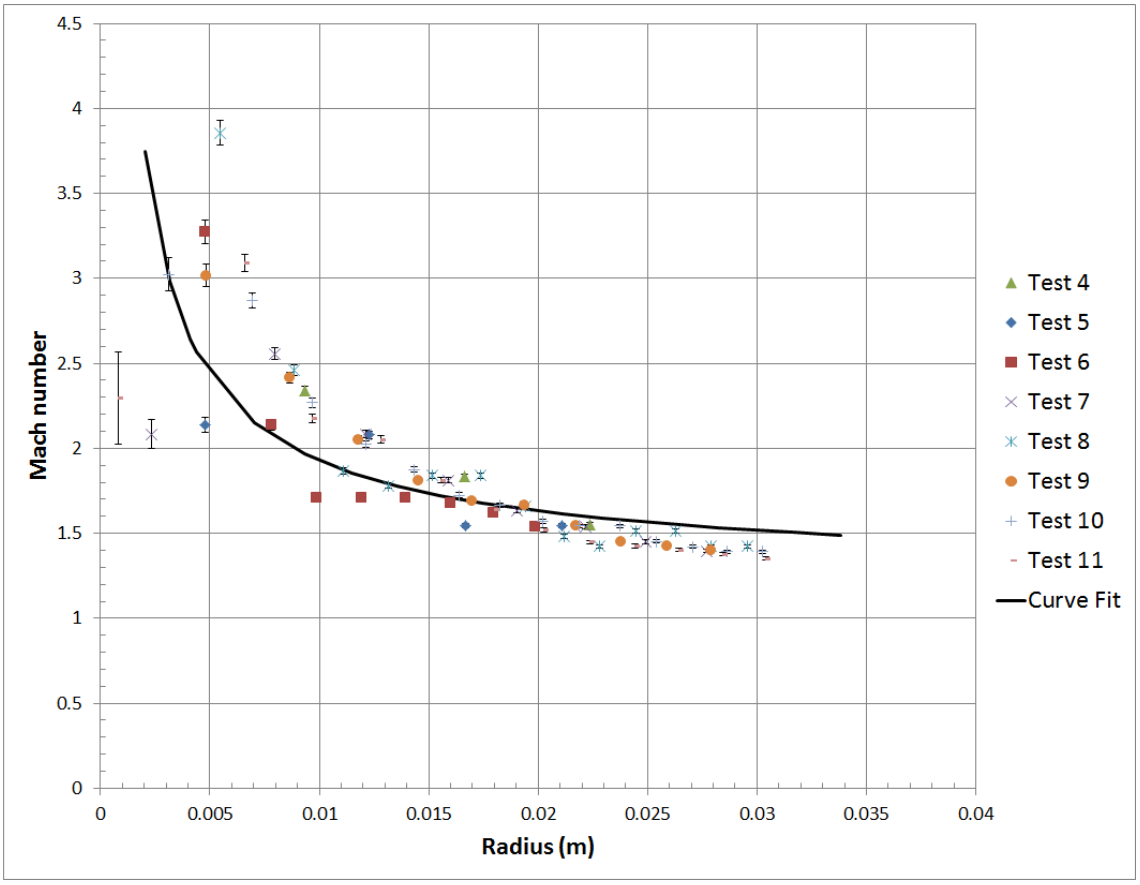

Figure 3.13: Near-field NONEL® tests, Mach number/radius

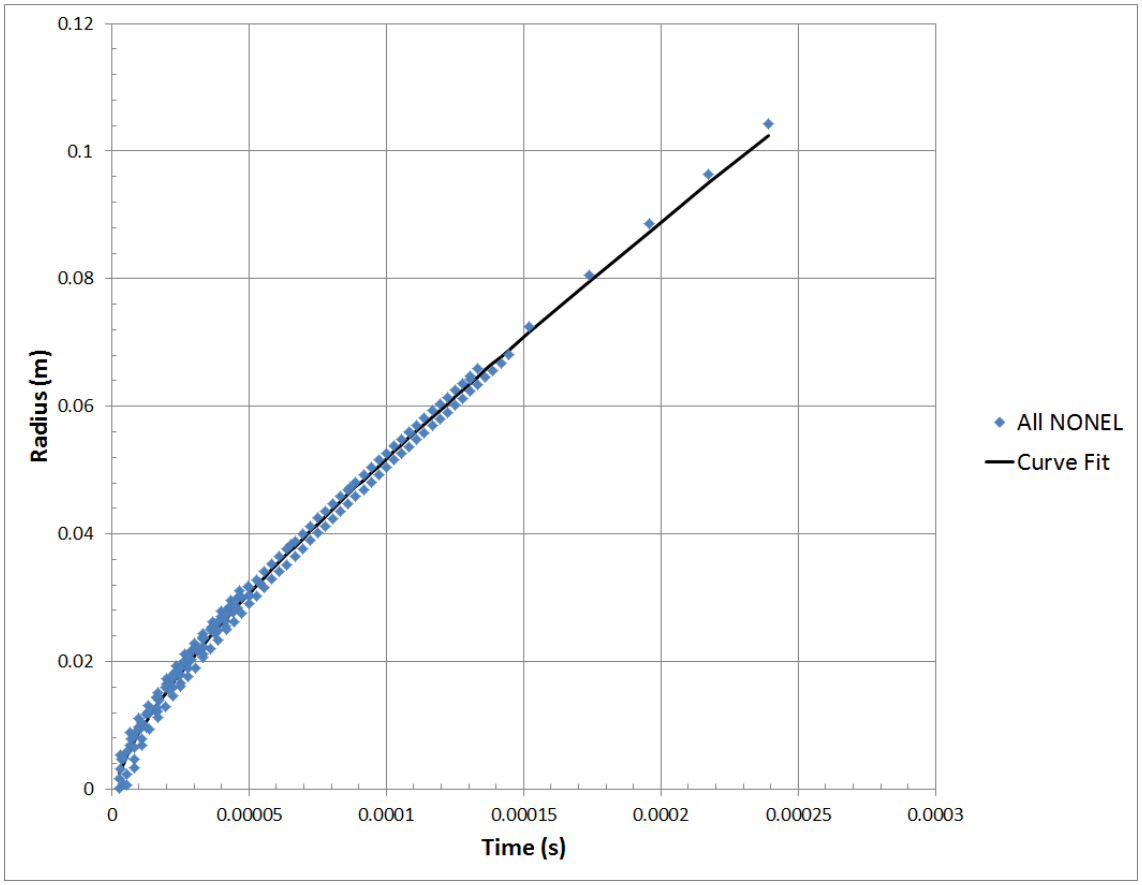

Figure 3.14: Graph of all NONEL® data

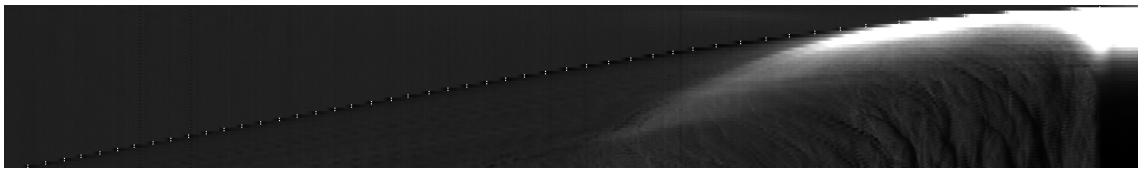

Figure 3.15: Streak image of a NONEL® test

streak image of the NONEL®, Figure 3.15. The shock front was assumed to be the leading edge of the fireball. The shock eventually becomes visible about 20 mm from the tip of the tube as it surpasses the fireball produced.

Secondly, the explosive in the tube is not solidly packed into the tube, nor is a solid; it is a powder and free to move about inside the tube. This is the reason that a propagation velocity is published rather than a detonation velocity. The calculated results for detonation velocity were less than half of this propagation velocity. It is surmised that since the shock tube only has a slight amount of explosive per foot and is basically hollow, that the energy lost to this air space inside the tube is the reason for such a difference between the detonation velocity of HMX and the propagation velocity.

Another problem with the explosive being a powder and free to move about in the tube is that the amount of explosive can vary along the length of the tube. This will affect the local propagation rate, so the rate at the end of the tube is not precisely known. The reported propagation value of 2100 m/s varies by as much as 15% ($\pm$ 300 m/s).

Lastly, the shock tube comes packaged in spools and has a natural curve to it because of this. Care was taken to try to remove this bend and keep the tip of the tube perpendicular to the camera and the ground as well, but this was not always the case. Also, since the lengths of tube were cut from the spool, care was also taken so that the face of the cut was at a 90 degree angle to the center axis. Were the cut not near a right angle, shock would exit at an undetermined angle from the end of the tube.

3.3 RP-2 Detonators

Four RP-2 detonators were fired and filmed at one million frames per second. Even at such a frame rate, the images were somewhat blurry due to the high speed of the shock front. Figure 3.16 shows a sequence of frames taken in one such test. Since the field of view is only about 40 millimeters, the shock front and the explosive product gases have not separated yet. The shock front, initially, will always be the leading event away from the initiation point. (Fragments accelerated by the explosion may eventually surpass the shock front, but no fragmentation was observed.) To calculate shock velocity, the leading pixel that could be defined as different from the background was taken as the leading

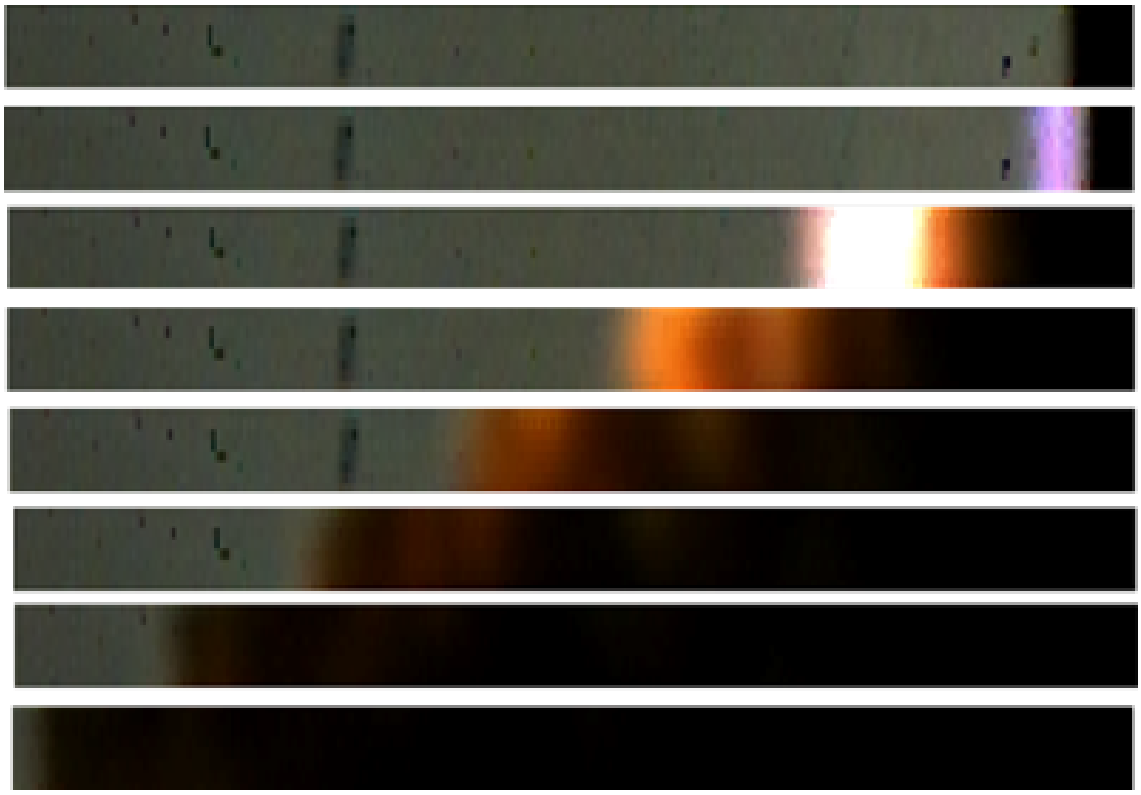

Figure 3.16: Sequential images of an RP2 detonator explosion filmed at one million frames per second. The scaled length of each photo is approximately 40 millimeters from end to end.

edge of the shock front. This includes both the light and dark leading edges in the frame sequence. Several blemishes on the background may be seen in the images, but do not alter the results in any way.

Density values for the explosives contained in the RP-2 detonators were obtained from the manufacturing company and reported to be 0.88 g/cc for the PETN and 1.6 g/cc for PBX-9407. Figure 2.13 in Chapter 2 shows the detonator contains PETN and RDX with a binder. While there are several formulas of plastically bonded explosives (PBXs), PBX-9407 happens to be 94% RDX and 6% of a fluoropolymer, FPC461 [8]. The published detonation velocity for PETN is 5.08 km/s and 7.91 for PBX-9407 at the given densities. [8][29] The expected detonation velocity would be closer to 7.91 km/s since the RDX is at the tip of the detonator.

To be sure the PBX is reaching steady state detonation and is not affected by the initiating PETN, the steady state run distance is calculated. Using the dimensions given in Figure 2.12 for the detonator and the density given, and assuming the thickness of the casing is about 0.5 mm, the depth of the PBX is calculated to be about 0.9 mm. The equation for initial shock pressure (P) to run distance (x) for PBX-9407 is [8]:

Table 3.1: Table of calculated RP-2 detonation velocities

Test	Interface Shock Velocity (km/s)	Detonation Velocity (km/s)
1	8.40	7.83
2	7.87	7.32
3	8.20	7.64
4	8.77	8.18
Average	8.31	7.74

$$logP = 0.57 - 0.49logx \text{ for } 1.4 < P < 4.7 \tag{3.2}$$

The CJ pressure for PETN is used for the pressure, P, and the run distance, x, is calculated to be 0.28 mm. Although, the CJ pressure for PETN (6.95 GPa) is outside of the range of pressures for the equation. Using the maximum pressure allowed (4.7 GPa), the run distance is found to be 0.62 mm. The higher actual pressure would shorten the run distance from this value. Even so, a run distance of 0.62 mm is shorter than the depth of the PBX in the detonator, so a steady state detonation is achieved. Therefore the expected detonation velocity value of 7.91 km/s is valid.

Figure 3.17 graphs the distance of the shock front versus time from detonation. Figure 3.18 shows the air shock velocity versus the distance from the RP-2 detonator face. Initial shock velocity at the explosive/air interface was extrapolated from the data in Figure 3.18 and was obtained using linear fit equations applied to the data sets. The y-intercept was then taken to be the velocity at the interface. The values ranged from 7.87 km/s to 8.77 km/s and had an average of 8.31 km/s. The detonation velocity was calculated for each test using the equations laid out in Chapter 2. The results are tabulated in Table 3.1.

The average detonation velocity calculated for the RP-2s was 7.74 $\pm$ 0.42 km/s. This is close to the published value for PBX-9407 (7.91 km/s) and within the uncertainty for the calculated value.

One interesting note, from the data in Table 3.1, is that the shock velocity is higher than the detonation velocity, which is not expected. Logic dictates that a shock will travel faster in a solid than in a gas, but that is not the case according to the results in this study, or the results in the work of Biss [4]. Confirmation of higher shock velocity using data for PBX9404 is shown below.

The Hugoniot for the pressure of the air at the interface is:

$$P_{air} = \rho_{air} C_0 u + \rho_{air} s u^2 \tag{3.3}$$

The equation for the pressure of the explosive at the interface is:

$$P_e = 235 P_{CJ} \frac{u}{u_{CJ}}^{-8.71} \tag{3.4}$$

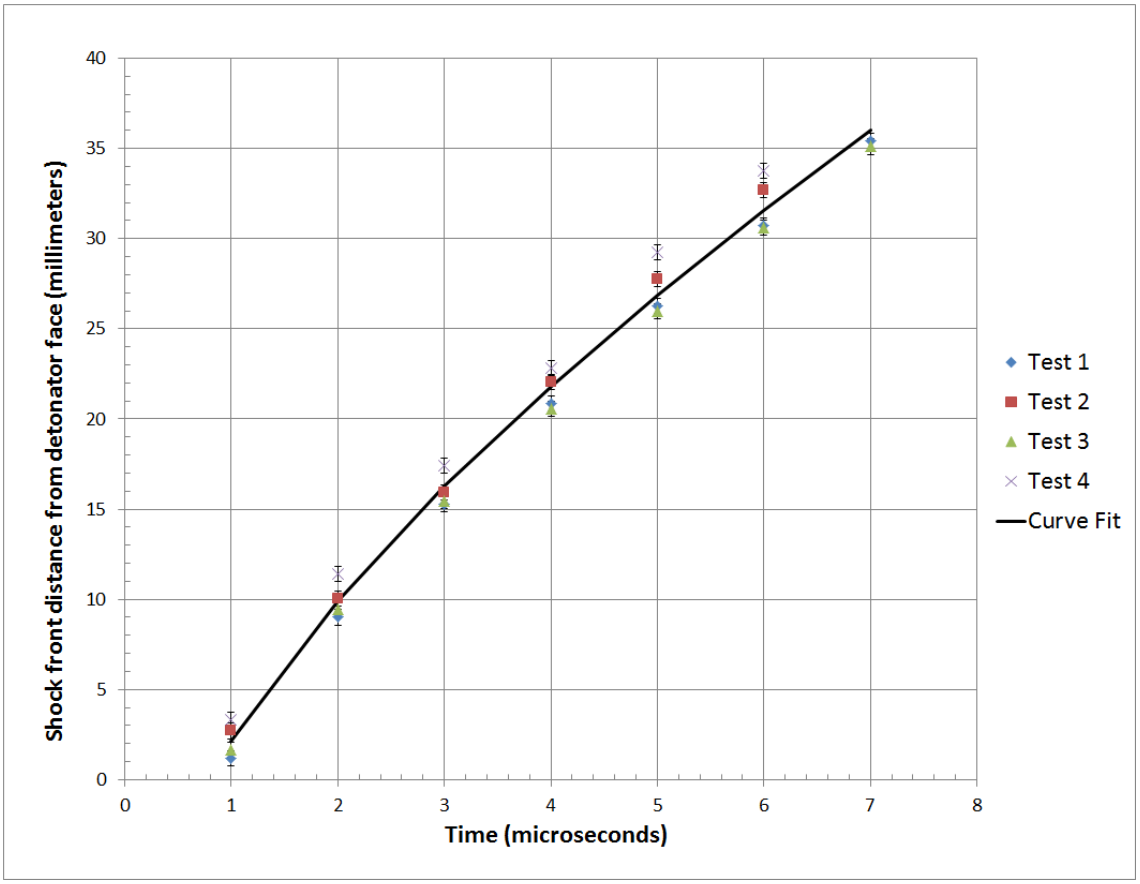

Figure 3.17: RP-2 radius/time graph

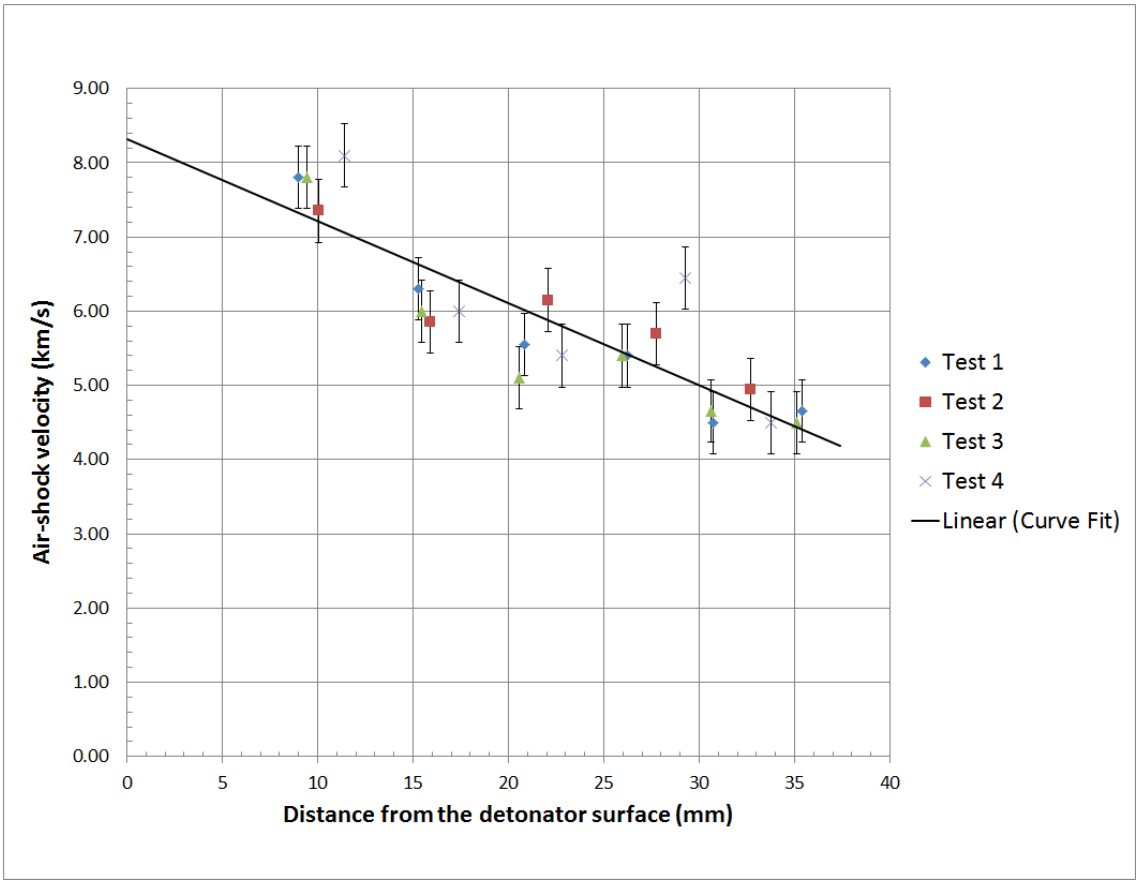

Figure 3.18: RP-2 shock velocity/radius graph

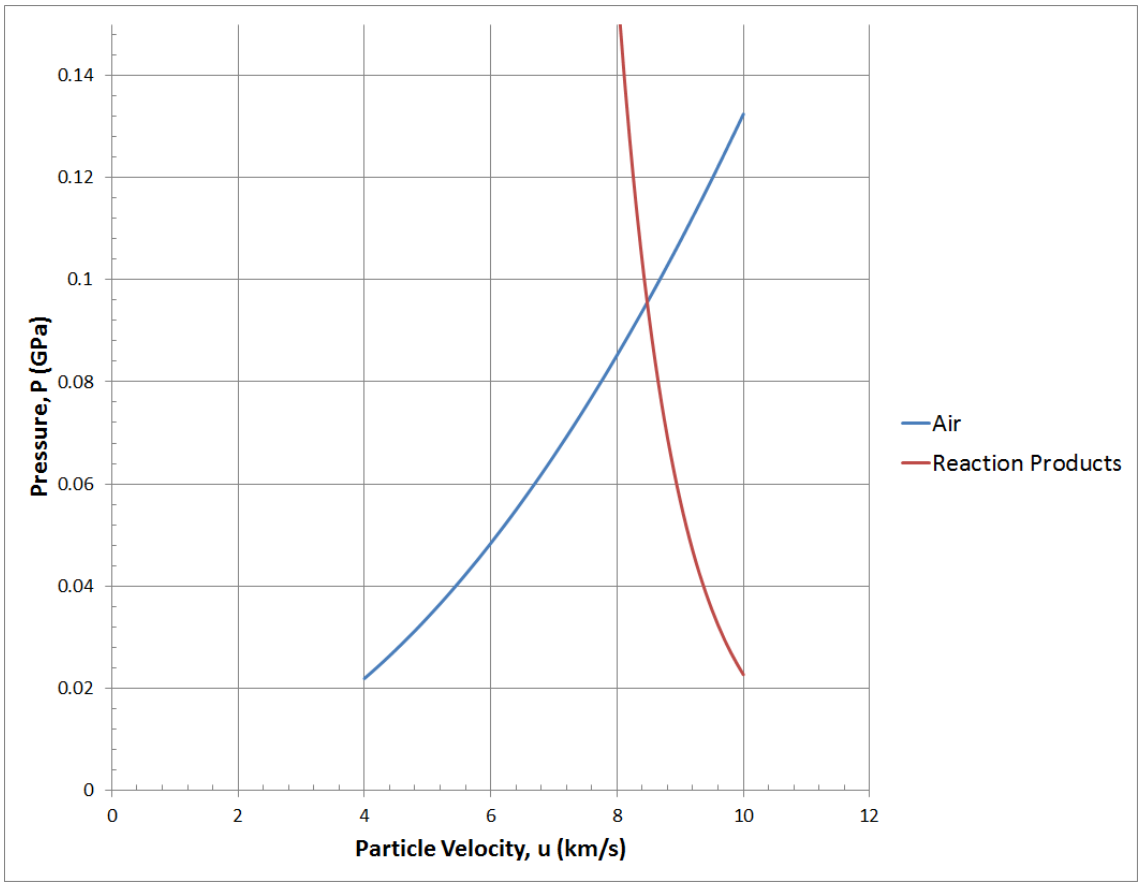

Figure 3.19: Interface interaction on the P - u Hugoniot plane

where

$$u_{CJ} = \frac{P_{CJ}}{\rho_e D} \tag{3.5}$$

We equate these two equations because the pressure must be the same at the interface.

Inserting the values for PBX9404 gives a particle velocity of u_{air} = 8.477 km/s which yields a shock velocity of U_{air} = 9.20 km/s which is indeed higher than the reported detonation velocity of 8.8 km/s. Figure 3.19 shows the graphical solution for equating the two pressure equations above. To be certain of the calculations, the values Biss [4] obtained for RDX were used in these equations as well and were consistent with that data.

3.4 Uncertainty Calculations

The main source of error in the calculation of shock velocity throughout the analysis of the entire study is the determination of the correct pixel for the shock front location. The MATLAB code [5] used to analyze the high-speed camera images contains code to calculate uncertainty for the output of radius and Mach number. The code for radius uncertainty uses the uncertainty of the shock location in pixels as well as the uncertainty of locating the edge of the calibration object in the calibration image in pixels. The Mach number uncertainty also takes into account a temperature uncertainty for determining the speed of sound in air. The uncertainties for shock location, calibration, and temperature used in all test analysis were 1 pixel, 2 pixels and 3 degrees Fahrenheit, respectively. Other uncertainties are listed by Biss [4], but it is reported that for all the properties calculated, the uncertainty is less than 2% and therefore omitted.

The uncertainty is affected by the number of pixels the shock travels in successive frames, and therefore changes from one frame to another. This is also true for the Mach number error. The uncertainties for both quantities for each frame were reported in the Excel output file. The error bars on all of the radius/time graphs are smaller than the symbols used to indicate the data points. Error bars for all Mach number/radius graphs are included.

The analysis for the RP-2 data was not done with the MATLAB code mentioned previously. The data was analyzed using Microsoft Excel and the error was subsequently calculated. The error bars in Figures 3.17 and 3.18 are based on an uncertainty in shock wave pixel position of $\pm$ 2 pixels due to more blur in the images and corresponds to $\pm$0.42 mm and $\pm$0.42 km/s, respectively. The uncertainty in measuring the calibration object resulted in an error accounting for less than 2% of the total error and was therefore deemed insignificant and omitted. No temperature uncertainty was calculated nor needed as the Mach number was not reported for the RP-2 tests.

CHAPTER 4

CONCLUSION AND FUTURE WORK

4.1 Conclusion

The available items to test this theory were not ideal. All the items tested emitted a shock wave from a cylindrical case, which directed the shock wave asymmetrically from the explosive/air interface. To get the most accurate shock wave velocity from testing cylindrical explosives, care must be taken to image the shock wave along the centerline axis of the cylinder. For a cylindrical explosive, the shock along the centerline axis is the only part of the detonation wave that does not experience side energy losses with sufficient diameter. Thus, the shock wave must be imaged along this same axis.

4.1.1 Shotgun shell primers

Testing for shotgun shell primers was inconclusive. Several problems arose while testing primers. While the active explosive ingredient in the primers is lead styphnate, there are other ingredients contained in the primer cup. These certainly affect the performance of the explosive, and to what degree is unknown. There are physical obstacles to overcome as well. A diagram of a primer is shown in Figure 4.1 [31].

A firing pin strikes the top of the primer cup, which compresses the impact sensitive compound onto an anvil contained within the primer. This ignites the primer compound which quickly converts to product gases. There is a small physical barrier at the end of the primer covering the flash hole to keep the compound contained within the cup (normally a thin piece of paper). The expansion of these gases must pass around the anvil, break the paper foil, then pass through a flash hole that is smaller than the diameter of the primer cup. All of these impedances extremely affect the emerging shock wave. Additionally, primers are made to ignite gun powder and not necessarily explode; therefore the amount of explosive compound contained in the primers may not be sufficient to produce a steady state detonation and only deflagrate.

Testing primers is easy, convenient, and inexpensive, and may be suited for other experiments. As for the scope of testing of this research, primers are not considered to be useful due to their construction and geometry.

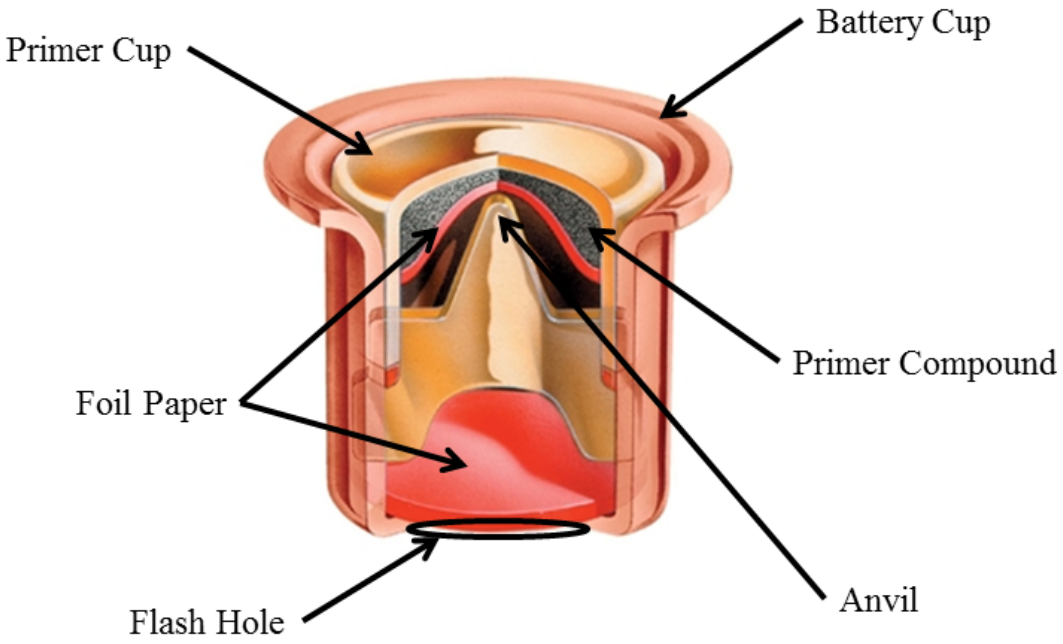

Figure 4.1: Schematic of shotgun shell primer

4.1.2 NONEL® Testing

NONEL® tests were inconclusive as well, and again there were several issues regarding the testing. Mainly, the problem of excessive light production for the explosive compound hindered locating of the shock front near the tip of the shock tube. Steps were taken to alleviate the problem, such as adding UV filters and stepping down the aperture on the camera lens, but the dilemma persisted.

Secondly, the compound in the shock tube is a powder and not solid throughout the length of the tube. The inside of the NONEL® is hollow with a small amount of the explosive powder coating the inside diameter plus some additional powder that is free to move about the length of the tube. This gives rise to the large variation (15%) in the manufacturers reported shock wave velocity. It would follow that the exiting shock wave would have a similar amount of variation. The reported shock velocity is also just a propagation rate and not a detonation value due to the air space. For this reason, determination of the detonation velocity of the compound contained in the shock tube does not seem feasible.

Shock tube is inexpensive and therefore advantageous to test. For the purpose of obtaining a detonation velocity of the explosive contents, the composition and performance limit the practicality of testing this product.

4.1.3 RP-2 Detonators

The detonation velocity results from testing the RP-2 detonators were very close to the actual published value for PBX-9407. This may be due to the fact that this was the only item tested that was pure in substance, solid in form, and was not impeded in any way from emerging from the end of the detonator. Testing was conducted with a very small field of view so that the shock wave was able to be imaged within the first few centimeters. The graph of the shock velocity versus radius was then nearly linear so that a fairly accurate interface velocity could be extrapolated.

4.2 Overall Observations

Composition of the item being tested seems to have the most relevance in this testing. To validate this method of detonation determination, the explosive compound should be in solid form and be of a well-known composition. Powders and explosive compounds mixed with other constituents did not test well.

Geometry and/or construction of the test item must be considered. The shock should be unimpeded at the explosive/air interface. Shot shell primers and shock tube do not appear to be suitable for testing. Detonators having cylindrical geometry may have merit, but more testing should be done to confirm this

assertion. Ideally, small spheres of pure explosives would best be suited for testing this method.

Care must be taken to get data as close as possible to the interface as possible. The shock wave decays rapidly during the first 30 millimeters for all items tested. Several data points must be taken during the rapid decay, before the shock decay tapers off near the asymptote of Mach 1. Many data points are needed to get the best curve fit and/or linear approximation to obtain the interface shock velocity value.

4.3 Future Work

Future work would include testing of spherical bare explosives on a small scale and/or on a larger scale if possible. Comparison between different size charges and the use of scaling laws could be explored. Spheres of explosives would safeguard that the shock wave would be uniform in all directions and therefore could be evaluated in any direction from the sphere. The testing ideally would include several different explosives. The problem of self-illumination must be addressed, as the fireball washes out the images in the first few microseconds, which is the critical part to investigate. Since there were a limited amount of tests completed with RP-2 detonators, more could be tested for further confirmation of results obtained in this study.

Most of the data collected from these experiments did not follow the idealized model of explosives (such as the ZND model). The shock velocity data acquired during these tests can be used in future work to obtain some useful information. The shock velocity can be used to calculate the particle velocity, and then the pressure at the explosive/air interface. While one cannot necessarily use the Rankine-Hugoniot equations for the explosive since it is not ideal, the Hugoniot equations still hold true for the air at the interface. The pressure data can them be used to determine if it is of sufficient magnitude to initiate another explosive.

REFERENCES

[1] U.S. Energy Information Administration. Energy explained, April 2013. http://www.eia.gov/energyexplained/index.cfm.

[2] Fickett, W., Davis, W. C. *Detonation: Theory and Experiment*. Dover Publications, Inc., 1979.

[3] M. H. Boyer. Calculation of Characteristics of Detonation Waves in Real Materials. *Journal of Applied Physics*, 40:654–661, 1969.

[4] M. M. Biss. Removing Full-scale Testing Barriers: Energetic Material Detonation Characterization at the Laboratory Scale. Technical Report ARL-TR-5943, Army Research Laboratory, 2012.

[5] M. J. Hargather. *Scaling, Characterization, and Application of Gram-Range Explosive Charges to Blast Testing of Materials*. PhD thesis, The Penn State University, 2008.

[6] G. S. Settles. *Schlieren and Shadowgraph Techniques: Visualizing Phenomena in Transparent Media*. Springer-Verlag, 2001.

[7] L. R. Rothstein. Predicting high explosives detonation velocities from their composition and structure. *Propellants and Explosives*, Vol. 6, 1981.

[8] P. W. Cooper. *Explosives Engineering*. Wiley-VCH, Inc., 1996.

[9] Kalmet, M. J., Jacobs, S. J. Chemistry of Detonations I, A Simple Method for Calculating Detonation Properties of CHNO Explosives. *Journal of Chemistry and Physics*, 48:23, 1968.

[10] Cooper, P. W., Kurowski, S. R. *Introduction to the Technology of Explosives*. Wiley-VCH, 1996.

[11] Persson, P., Holmberg, R., Lee, J. *Rock Blasting and Explosives Engineering*. CRC Press LLC, 1994.

[12] C. L. Mader. *Numerical modeling of Explosive and Propellants*. CRC Press, 3rd edition, 2008.

[13] Dorsett H. E. Cliff M. D. Anderson J. C. Brousseau, P. Detonation propperties of explosives containing nanometric aluminum powder. 2002.

[14] P. W. Cooper. Comments on TNT equivalence. In *20th International Pyrotechnics Seminar*, 1994.

[15] Benterou, J., Bennett, C.V., Cole, G., Hare, D. E., May, C., Udd, E. Internal Detonation Velocity Measurements Inside High Explosives. Technical Report LLNL-PROC-409969, Lawrence Livermore National Laboratory, 2009.

[16] Netherwood, P. H. Jr. Detonation Velocity Measurements of the Explosives Detasheet C and Amatol. Technical Report BRL-MR-3427, US Army Ballistic Research Laboratory, 1985.

[17] Gustavsen, R.L., Sheffield, S.A., Alcon, R.R. Progress in Measuring Detonation Wave Profiles in PBX9501. Technical Report LA-UR-98-3781, Los Alomos National Laboratory, 1999.

[18] D.B. Holtkamp. Photonic Doppler Velocimetry for Dynamic Experiments. Technical Report LA-UR-11-05790, Los Alomos National Laboratory, 2011.

[19] C. R. Nave. Refraction of Light, Index of Refraction, Snell's Law. website, 2012. http://hyperphysics.phy-astr.gsu.edu/hbase/geoopt/refr.html.

[20] Hamamatsu Photonics. Guide to Streak Cameras, 2008. http://www.hamamatsu.com/resources/pdf/sys/e_streakh.pdf.

[21] L. Hardesty. Trillion-frame-per-second video, December 2011. http://web.mit.edu/newsoffice/2011/trillion-fps-camera-1213.html.

[22] R. Hooke. *Micrographia, "Of a New Property in the Air,"*. 1665.

[23] Hargather, M. J., Settles, G.S. Retroreflective shadowgraph technique for large-scale flow visualization. *Applied Optics*, 48:4449–4457, 2009.

[24] Hargather, M. J., Settles, G. S. Background-oriented schlieren visualization of heating and ventilation flows. *HVAC&R Research*, 17:771–780, 2011.

[25] Obed SI, Jagadeesh G, and Kontis K. Micro-blast waves using detonation transmission tubing. In *Proceedings of the 27th International Symposium on Shock Waves*, 2009.

[26] Teledyne Technology, Inc. RP-2 EBW Detonator, 2011. http://www.teledynerisi.com/productpdf/page21.pdf.

[27] Remington Arms. Material Safety Data Sheet Product: Component Empty Shellcases (Primed) (Shotshell), October 2001. http://www.remington.com/products/ammunition/components/shotshell-components /shotshellprimers.aspx.

[28] J. Akhavan. *The Chemistry of Explosives*. Royal Society of Chemistry Publishing, 3rd edition, 2011.

[29] Dobratz, B.M., Crawford, P. C. LNLL Explosives Handbook, Properties of Chemical Explosives and Explosive Simulants. Handbook, 1985. Lawrence Livermore National Laboratory.

[30] J.M. Dewey. *Handbook of Flow Visualization*. Hemisphere Publishing Corp., 1st edition, 1989.

[31] Edgar Brothers Shooting Sports. Primer image, 2014. http://shootingsports.edgarbrothers.com/pages/Primers_1.aspx.

DETERMINATION OF DETONATION VELOCITY OF EXPLOSIVE COMPOUNDS USING OPTICAL TECHNIQUES

by

Michael Scott Shattuck